A promoter interaction map for cardiovascular disease genetics

Lindsey E. Montefiori[1], Débora R. Sobreira[1], Noboru J. Sakabe[1], Ivy Aneas[1], Amelia C. Joslin[1], Grace T. Hansen[1], Grazyna Bozek[1], Ivan P. Moskowitz[1,2], Elizabeth M. McNally[3], Marcelo A. Nóbrega[1]

[1]Department of Human Genetics, The University of Chicago, Chicago IL; [2]Department of Pediatrics and Pathology, The University of Chicago, Chicago IL; [3]Center for Genetic Medicine, Northwestern University Feinberg School of Medicine, Chicago IL

Address for Correspondence:

Marcelo A. Nóbrega
Department of Human Genetics
920 E. 58th St.
CLSC Room 515
773-702-1808
Email: nobrega@uchicago.edu

Lindsey Montefiori
Department of Human Genetics
920 E 58th St.
CLSC Room 515
773-702-1808
Email: lem@uchicago.edu

Abstract

Over 500 genetic loci have been associated with risk of cardiovascular diseases (CVDs), however most loci are located in gene-distal non-coding regions and their target genes are not known. Here, we generated high-resolution promoter capture Hi-C (PCHi-C) maps in human induced pluripotent stem cells (iPSCs) and iPSC-derived cardiomyocytes (CMs) to provide a resource for identifying and prioritizing the functional targets of CVD associations. We validate these maps by demonstrating that promoters preferentially contact distal sequences enriched for tissue-specific transcription factor motifs and are enriched for chromatin marks that correlate with dynamic changes in gene expression. Using the CM PCHi-C map, we linked 1,999 CVD-associated SNPs to 347 target genes. Remarkably, more than 90% of SNP-target gene interactions did not involve the nearest gene, while 40% of SNPs interacted with at least two genes, demonstrating the importance of considering long-range chromatin interactions when interpreting functional targets of disease loci.

Introduction

A major goal in human genetics research is to understand genetic contributions to complex diseases, specifically the molecular mechanisms by which common DNA variants impact disease etiology. Most genome-wide association studies (GWAS) implicate non-coding variants that are far from genes, complicating interpretation of their mode of action and correct identification of the target gene (Maurano et al. 2012). Mounting evidence suggests that disease variants disrupt the function of *cis*-acting regulatory elements, such as enhancers, which in turn affects expression of the specific gene or genes that are functional targets of these elements (Wright et al. 2010; Musunuru et al. 2010; Cowper-Sal·lari et al. 2012; Smemo et al. 2014; Claussnitzer et al. 2015). However, because *cis*-acting regulatory elements can be located kilobases (kb) away from their target gene(s), identifying the true functional targets of regulatory elements remains challenging (Smemo et al. 2014).

Chromosome conformation capture techniques such as Hi-C (Lieberman-Aiden et al. 2009) enable the genome-wide mapping of long-range chromatin contacts and therefore represent a promising strategy to identify distal gene targets of disease-associated genetic variants. Recently, Hi-C maps have been generated in numerous human cell types including embryonic stem cells and early embryonic lineages (Dixon et al. 2012, 2015), immune cells (Rao et al. 2014), fibroblasts (Jin et al. 2013) and other primary tissue types (Schmitt et al. 2016). However, despite the increasing abundance of Hi-C maps, most datasets are of limited resolution (>40 kb) and do not precisely identify the genomic regions in contact with gene promoters.

More recently, promoter capture Hi-C (PCHi-C) was developed which greatly increases the power to detect interactions involving promoter sequences (Schoenfelder et al. 2015; Mifsud et al. 2015). PCHi-C in different cell types identified thousands of enhancer-promoter contacts and revealed extensive differences in promoter architecture between cell types and throughout differentiation (Schoenfelder et al. 2015; Mifsud et al. 2015; Javierre et al. 2016; Freire-Pritchett et al. 2017; Rubin et al. 2017; Siersbæk et al. 2017). These studies collectively demonstrated that genome architecture

reflects cell identity, suggesting that disease-relevant cell types are critical for successful interrogation of the gene regulatory mechanisms of disease loci.

In support of this notion, several recent studies utilized high-resolution promoter interaction maps to identify tissue-specific target genes of GWAS associations. Javierre *et al*. generated promoter capture Hi-C data in 17 primary human blood cell types and identified 2,604 potentially causal genes for immune- and blood-related disorders, including many genes with unannotated roles in those diseases (Javierre et al. 2016). Similarly, Mumbach *et al*. interrogated GWAS SNPs associated with autoimmune diseases using HiChIP where they identified ~10,000 promoter-enhancer interactions that linked several hundred SNPs to target genes, most of which were not the nearest gene (Mumbach et al. 2017). Importantly, both studies reported cell-type specificity of SNP-target gene interactions.

Cardiovascular diseases, including cardiac arrhythmia, heart failure, and myocardial infarction, continue to be the leading cause of death world-wide. Over 50 GWAS have been conducted for these specific cardiovascular phenotypes alone, with more than 500 loci implicated in cardiovascular disease risk (NHGRI GWAS catalog, https://www.ebi.ac.uk/gwas/), most of which map to non-coding genomic regions. To begin to dissect the molecular mechanisms by which genetic variants contribute to CVD risk, a comprehensive gene regulatory map of human cardiac cells is required. Here, we present high resolution promoter interaction maps of human iPSCs and iPSC-derived cardiomyocytes (CMs). Using PCHi-C, we identified hundreds of thousands of promoter interactions in each cell type. We demonstrate the physiological relevance of these datasets by functionally interrogating the relationship between gene expression and long-range promoter interactions, and demonstrate the utility of long-range chromatin interaction data to resolve the functional targets of disease-associated loci.

Results

iPSC-derived cardiomyocytes provide an effective model to study the architecture of CVD genetics

We used iPSC-derived CMs (Burridge et al. 2014) as a model to study cardiovascular gene regulation and disease genetics. The CMs generated in this study were 86-94% pure based on cardiac Troponin T protein expression and exhibited spontaneous, uniform beating (Figure 1—figure supplement 1A, Supplementary Mov. 1). To demonstrate that iPSCs and CMs recapitulate transcriptional and epigenetic profiles of matched primary cells, we conducted RNA-seq and ChIP-seq for the active enhancer mark H3K27ac in both cell types and compared these data with similar cell types from the Epigenome Roadmap Project (Roadmap Epigenomics Consortium et al. 2015). RNA-seq profiles of iPSCs clustered tightly with H1 embryonic stem cells, whereas CMs clustered with both left ventricle (LV) and fetal heart (FH) profiles (Figure 1—figure supplement 1B). Furthermore, we observed that matched cell types exhibited three-fold greater overlap in the number of promoter-distal H3K27ac ChIP-seq peaks than non-matched cell types (Figure 1—figure supplement 1C,D), indicating that both iPSCs and CMs recapitulate tissue-specific epigenetic states of human stem cells and primary cardiomyocytes, respectively.

To further validate our system, we analyzed differentially expressed genes between iPSCs and CMs. Among the top 10% of over-expressed genes in CMs were genes directly related to cardiac function including essential cardiac transcription factors (*GATA4*, *MEIS1*, *TBX5*, and *TBX20*) and differentiation products (*TNNT2*, *MYH7B*, *MYL7*, *ACTN2*, *NPPA*, *HCN4*, and *RYR2*) (fold-change > 1.5, $P_{adj} < 0.05$, Figure 1—figure supplement 2A-C). Gene Ontology (GO) enrichment analysis for genes over-expressed in CMs relative to iPSCs further confirmed the cardiac-specific phenotypes of these cells with top terms relating to the development of the cardiac conduction system and cardiac muscle cell contraction (Figure 1—figure supplement 2D).

Promoter-capture Hi-C identifies distal regulatory elements in iPSCs and CMs

To comprehensively map long-range regulatory elements in iPSCs and CMs, we performed *in-situ* Hi-C (Rao et al. 2014) in triplicate iPSC-CM differentiations; importantly, we used the 4-cutter restriction enzyme MboI which generates ligation fragments with an average size of 422 bp, enabling

enhancer-level resolution of promoter contacts. We enriched iPSC and CM *in situ* Hi-C libraries for promoter interactions through hybridization with a set of 77,476 biotinylated RNA probes ("baits") targeting 22,600 human RefSeq protein-coding promoters (see Methods) and sequenced each library to an average depth of ~413 million (M) paired-end reads. After removing duplicates and read-pairs that did not map to a bait, we obtained an average of 31M and 41M read-pairs per replicate for iPSC and CM, respectively. We used CHiCAGO (Cairns et al. 2016), a computational pipeline which accounts for bias from the sequence capture, to identify significant interactions and further filtered for those significant in at least two out of three replicates (see Methods). Finally, we exclusively focused on interactions that were separated by a distance of at least 10 kb. This criterion addresses the high frequency of close-proximity ligation evets in Hi-C data, which are difficult to distinguish as random Brownian contacts or functional chromatin interactions (Cairns et al. 2016). In total, we identified 350,062 promoter interactions in iPSCs and 401,098 in CMs. A large proportion (~55%) of interactions were shared between the two cell types, indicating that even at high resolution many long-range interactions are stable across cell types (Figure 1A). Approximately 20% of all interactions were between two promoters, demonstrating the high connectivity between genes and supporting the recently suggested role of promoters acting as regulatory inputs for distal genes (Dao et al. 2017; Diao et al. 2017) (Figure 1B). Most interactions were promoter-distal, with a median of ~170 kb between the promoter and the distal-interacting region (Figure 1C).

To compare the PCHi-C maps with known features of genome organization, we sequenced our pre-capture Hi-C libraries to an average depth of 665M reads per cell type and identified topologically associating domains (TADs) with TopDom (see Methods). TADs are organizational units of chromosomes defined by <1 megabase (Mb) genomic blocks that exhibit high self-interacting frequencies with a very low interaction frequency across TAD boundaries (Dixon et al. 2012; Nora et al. 2012). Notably, this organization is thought to constrain the activity of *cis*-regulatory elements to target genes with the same TAD, as disruption of TAD boundaries has been shown to lead to aberrant

activation of genes in neighboring TADs (Nora et al. 2012; Lupiáñez et al. 2015; Franke et al. 2016; Symmons et al. 2016; Tsujimura et al. 2015). We found that the majority of PCHi-C interactions occurred within TADs (73% and 77% in iPSCs and CMs, respectively; Figure 1D and Figure 1—figure supplement 3A). TAD-crossing interactions ("inter-TAD") contained proportionally more promoter-promoter interactions than intra-TAD interactions, and were more likely to overlap promoter-distal CTCF sites; however, they were similarly enriched for looping to distal H3K27ac sites, a mark of active chromatin (Figure 1—figure supplement 3B-D). Inter-TAD interactions had slightly lower CHiCAGO scores, reflecting a lower number of reads supporting these interactions, and spanned greater genomic distances than intra-TAD interactions (Figure 1—figure supplement 3E,F). Additionally, promoters with inter-TAD interactions were preferentially located close to TAD boundaries (Figure 1—figure supplement 3G) and had higher expression levels compared to promoters with intra-TAD interactions, particularly in CMs (Figure 1—figure supplement 3H). These observations are consistent with previous studies which demonstrated that highly expressed genes, specifically housekeeping genes, are enriched at TAD boundaries (Dixon et al. 2012).

To illustrate the utility of high-resolution PCHi-C interaction maps, we highlight the *GATA4* locus in Figures 1D and 1E. *GATA4* is a master regulator of heart development (Watt et al. 2004; Pikkarainen et al. 2004) and the *GATA4* gene is located in a TAD structure that is relatively stable between iPSCs and CMs (Figure 1D). However, PCHi-C identified increased interaction frequencies between the *GATA4* promoter and several H3K27ac-marked regions, including four *in vivo* validated heart enhancers from the Vista enhancer browser (Visel et al. 2007), specifically in CMs and coincident with strong up-regulation of *GATA4* (Figure 1 – figure supplement 2C). Although TAD-based analyses help define a gene's *cis*-regulatory landscape, high resolution promoter interaction data provides the resolution necessary to precisely map enhancer-promoter interactions in the context of cellular differentiation.

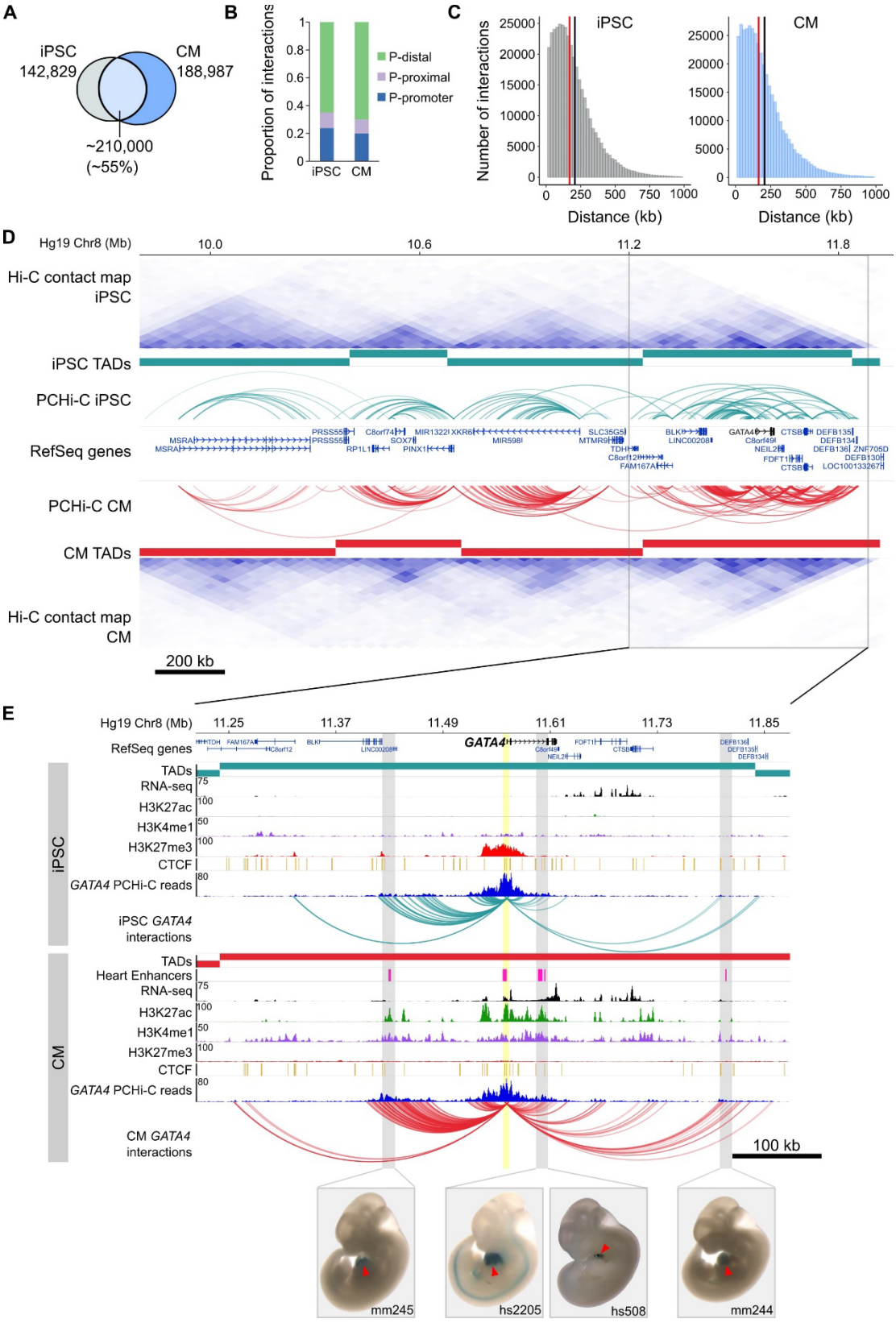

Figure 1. General features of promoter interactions. (A) Venn diagram displaying the number of cell type-specific and shared promoter interactions in each cell type. **(B)** Proportion of interactions in each distance category: promoter (P)-promoter (both interacting ends overlap a transcription start site (TSS)); P-proximal (non-promoter end overlaps captured region but not the TSS); P-distal (non-promoter end is outside of captured region). Note that all promoter interactions are separated by at least 10 kb. **(C)** Distribution of the distances spanning each interaction in iPSCs and CMs. The red line depicts the median (170 kb in iPSCs, 164 kb in CMs); the black line depicts the mean (208 kb in iPSCs, 206 kb in CMs). **(D)** A ~2 Mb region of chromosome 8 encompassing the *GATA4* gene is shown along with pre-capture (whole genome) Hi-C interaction maps at 40 kb resolution for iPSCs (top) and CMs (bottom). TADs called with TopDom are shown as colored bars (median TAD size = 640 kb in both cell types, mean TAD size = 742 kb in iPSCs and 743 kb in CMs) and significant PCHi-C interactions as colored arcs. **(E)** Zoomed-in view of the *GATA4* locus (promoter highlighted in yellow) in iPSCs (top) and CMs (bottom) along with corresponding RNA-seq data generated as part of this study, and ChIP-seq data for H3K27ac, H3K4me1, H3K27me3 and CTCF from the Epigenome Roadmap Project/ENCODE (H1 and left ventricle for iPSC and CM, respectively). Filtered *GATA4* read counts used by CHiCAGO are displayed in blue with the corresponding significant interactions shown as arcs. For clarity, only *GATA4* interactions are shown. Gray highlighted regions show interactions overlapping *in vivo* validated heart enhancers (pink boxes), with representative E11.5 embryos for each enhancer element (Visel et al. 2007). Red arrowhead points to the heart.

To validate the CM interaction map as a resource for cardiovascular disease genetics we next extensively characterized several important aspects of genetic architecture in CMs. We compared CMs with iPSCs in each analysis as a measure of cell-type specificity. These analyses serve as benchmarks that build on established features of genome organization and aid interpretations of the roles that long range interactions play in gene regulation.

Promoter interactions are enriched for tissue-specific transcription factor motifs

Distal enhancers activate target genes through DNA looping, a mechanism that enables distally bound transcription factors to contact the transcription machinery of target promoters (Pennacchio et al. 2013; Miele and Dekker 2008; Deng et al. 2012). To assess whether this feature of gene regulation was reflected in the iPSC and CM interactions, we conducted motif analysis using HOMER (Heinz et al. 2010) on the set of promoter-distal interacting sequences in each cell type. We initially focused on interactions for genes differentially expressed between iPSCs and CMs (fold-change > 1.5, $P_{adj} < 0.05$).

We identified CTCF as the most enriched motif in each case (Figures 2A,B), consistent with the known role of this factor in mediating long-range genomic interactions (Phillips and Corces 2009; Phillips-Cremins et al. 2013; Nora et al. 2017). Among the other top motifs, we identified the pluripotency factor motifs OCT4-SOX2-TCF-NANOG (OSN) and SOX2 as preferentially enriched in distal sequences looping to genes over-expressed in iPSCs (Figures 2A,C), whereas top motifs in distal sequences looping to genes over-expressed in CMs included TBX20, ESRRB and MEIS1 (Figures 2B,C). TBX20 and MEIS1 transcription factors are important regulators of heart development and function (Cai et al. 2005; Sakabe et al. 2012; Mahmoud et al. 2013) and ESRRB was previously identified as a potential binding partner of TBX20 in adult mouse cardiomyocytes (Shen et al. 2011). We also observed that distal interactions unique to either iPSCs or CMs were similarly enriched for tissue-specific transcription factor motifs (Figure 2D). In line with a recent report that AP-1 contributes to dynamic loop formation during macrophage development (Phanstiel et al. 2017), both iPSC- and CM-specific interactions were enriched for AP-1 motifs (Figure 2D), suggesting that AP-1 transcription factors may represent a previously unrecognized genome organizing complex.

A

Motif	Logo	% sites	Rank	P-value
CTCF		4.85%	1	1 x 10^{-107}
OSN		6.51%	3	1 x 10^{-20}
SOX2		22.46%	6	1 x 10^{-14}
OCT4		13.30%	31	1 x 10^{-8}

B

Motif	Logo	% sites	Rank	P-value
CTCF		4.59%	1	1 x 10^{-100}
TBX20		6.46%	8	1 x 10^{-20}
ESRRB		17.7%	16	1 x 10^{-18}
MEIS1		41.06%	24	1 x 10^{-16}

C

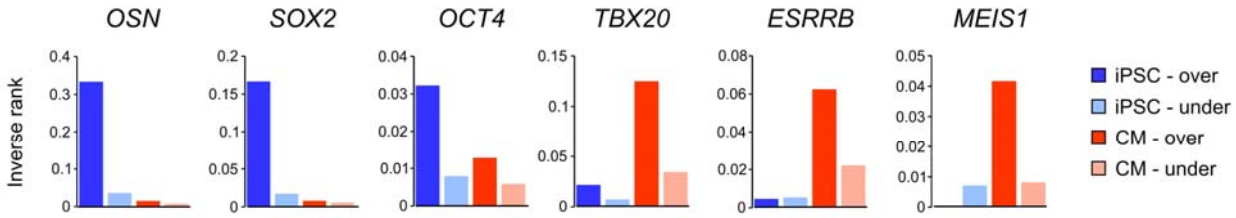

D

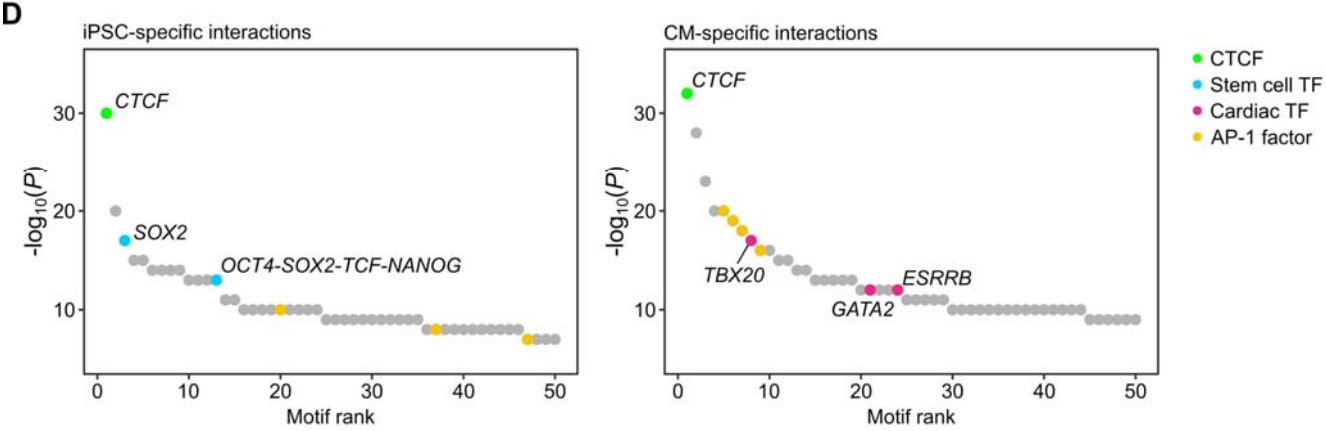

Figure 2. Transcription factor motif enrichment in distal interacting regions. (A,B) Selected transcription factor (TF) motifs identified using HOMER in the promoter-distal interacting sequences for all over-expressed genes in **(A)** iPSCs and **(B)** CMs (fold change > 1.5, P_{adj} < 0.05). "% sites" refers to the percent of distal interactions overlapping the motif; rank is based on P-value significance. **(C)** To compare motif ranks across gene sets, the inverse of the rank is plotted for selected motifs identified in distal interactions from over- or under-expressed genes in both iPSCs and CMs. **(D)** The top 50 motifs identified in cell type-specific interactions. *OSN*, OCT4-SOX2-TCF-NANOG motif.

Long-range promoter interactions are enriched for active *cis*-regulatory elements and correspond to gene expression dynamics

Functionally active *cis*-regulatory elements are characterized by the presence of specific histone modifications; active enhancers are generally associated with H3K4me1 and H3K27ac (Creyghton et al. 2010; Heintzman et al. 2009), whereas inactive (e.g. poised or silenced) elements are often associated with H3K27me3 (Rada-Iglesias et al. 2011; Erceg et al. 2017). In support of the gene-regulatory function of long-range interactions, we found that the promoter-distal MboI fragments involved in significant promoter interactions were enriched for these three histone modifications in both iPSCs and CMs (Figures 3A-C). When promoters were grouped by expression level, we observed that this enrichment increased with increasing expression for H3K27ac and H3K4me1, and decreased with increasing expression for H3K27me3, consistent with an additive nature of enhancer-promoter interactions (Schoenfelder et al. 2015; Javierre et al. 2016), and validating that PCHi-C enriches for likely functional long-range chromatin contacts.

A strong correlation (Pearson correlation coefficient $r > 0.7$) between the degree of histone modifications and gene expression was first reported nearly ten years ago (Karlić et al. 2010), however that analysis only considered histone modifications within 2 kb of promoters. To understand whether this relationship extends beyond promoter-proximal regions, we correlated the number of histone ChIP-seq peaks within 300 kb of promoters with the promoter's expression level (Figure 3—figure supplement 1A,B). H3K27ac and H3K4me1 both positively correlated with expression level (Spearman's $\rho = 0.22$ and 0.16, respectively in iPSC and $\rho = 0.23$ and 0.24, respectively in CMs, $P < 2.2^{-16}$); in contrast, H3K27me3 negatively correlated with expression level in CMs (Spearman's $\rho = -0.20$, $P < 2.2^{-16}$), however this relationship was not present in iPSCs (Spearman's $\rho = 0.02$, $P = 0.06$). Although moderate, these correlations could partially explain why higher expressed genes show stronger enrichment for promoter interactions overlapping histone peaks when using a genome-wide background model (see Methods), and lends support to the notion that active genes are located in generally active genomic environments (Stevens et al. 2017; Gilbert et al. 2004).

We next investigated the relationship between cell type-specific interactions and enrichment for tissue-specific CTCF, H3K27ac, and H3K27me3 marks, hypothesizing that interactions unique to iPSCs or CMs would be most enriched for tissue-specific chromatin features. Indeed, we observed that cell type-specific interactions preferentially involved H3K27ac peaks from the matched cell type, and were either not enriched (iPSC) or depleted (CM) for H3K27ac marks that were specific to the non-matched cell type (Figure 3E, middle panel). However, the strongest enrichment was for cell type-specific interactions to overlap chromatin features that were present in both cell types (Figure 3E). Additionally, interactions that were shared between iPSCs and CMs were most enriched for shared chromatin features. These results suggest that all interactions, whether shared or unique to one cell type, preferentially contact regulatory regions that are active in both cell types, whereas cell type-specific interactions are not likely to occur in regions specifically marked in the non-matched cell type.

An example of a gene that encompasses these observations is the atrial natriuretic peptide gene *NPPA* (Figure 3F) which is specifically expressed in cells of the heart atrium and is upregulated in CMs (Figure 1—figure supplement 2C). *NPPA* makes numerous cell type-specific interactions to a distal region that is only marked with active chromatin (H3K27ac and H3K4me1) in CMs; furthermore, functional characterization showed that this region corresponds to an *in vivo* enhancer recapitulating *NPPA*'s endogenous expression in the developing heart (Visel et al. 2007). Taken together, these results illuminate the complex relationship between long-range promoter interactions and gene regulation and provide evidence that promoter architecture reflects cell type-specific gene expression.

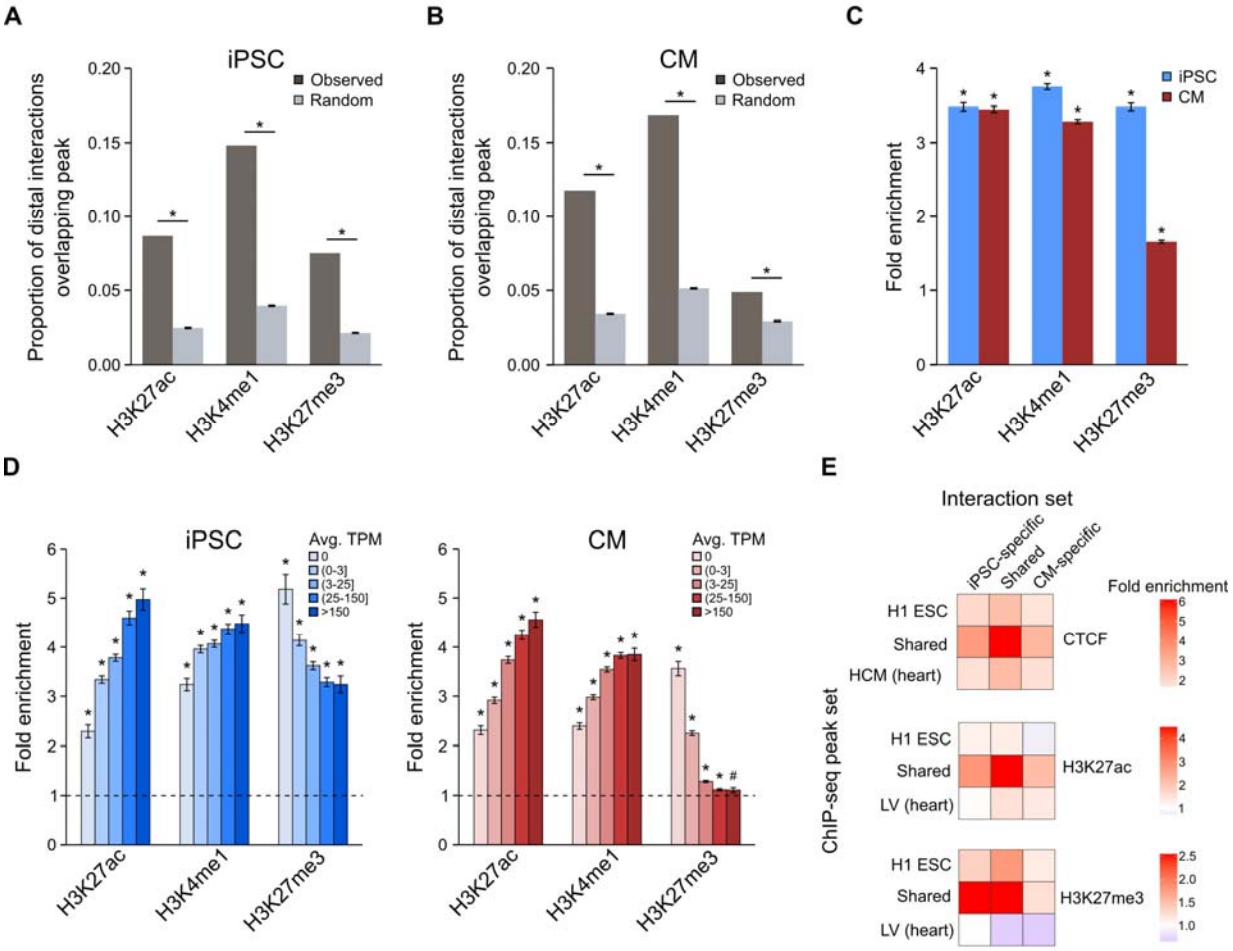

284

Figure 3. Enrichment of promoter interactions to distal regulatory features. (A,B) Proportion of promoter-distal interactions overlapping a histone ChIP-seq peak compared to random control MboI fragments (see Methods). iPSC interactions were overlapped with H1 ESC ChIP-seq data; CM interactions were overlapped with left ventricle ChIP-seq data from the Epigenome Roadmap Project (Supplementary File 10). **(C)** Fold enrichment of the data presented in **(A)** and **(B)**. **(D)** Fold enrichment of promoter-distal interactions based on the expression level of the promoter. Promoters were grouped into 5 bins according to their average TPM values. Dashed line indicates no enrichment. **(E)** Fold enrichment of cell type-specific and shared interactions (columns) to tissue-specific and shared chromatin features (rows). **(F)** Example of the *NPPA* gene in iPSCs (top) and CMs (bottom). Gray box highlights CM-specific interactions to CM-specific chromatin marks and an *in vivo* heart enhancer (Visel et al. 2007). For clarity, only interactions for *NPPA* are shown. **P* < 0.00001, $^{\#}$P = 0.0017, Z-test.

Dynamic changes in genomic compartmentalization involve a subset of cardiac-specific genes

As a final benchmark of our datasets, we analyzed large-scale differences in genome organization between iPSCs and CMs. The first Hi-C studies revealed that the genome is organized in two major compartments, A and B, that correspond to open and closed regions of chromosomes, respectively (Lieberman-Aiden et al. 2009; Rao et al. 2014). Although most compartments are stable across different cell types, some compartments switch states in a cell type-specific manner which may reflect important gene regulatory changes (Dixon et al. 2015). To assess whether capture Hi-C data, which is more cost-effective for capturing promoter-centered interactions, is able to identify A/B compartments, we compared our capture Hi-C data with pre-capture, genome-wide Hi-C libraries. A/B compartments identified using HOMER (Heinz et al. 2010) were remarkably similar in the whole-genome and PCHi-C datasets (97% correspondence, Figure 4A, top panel, and Figure 4—figure supplements 1 and 2), demonstrating that PCHi-C data contains sufficient information to identify broadly active and inactive regions of the genome. As an example, we highlight a 10 Mb region on chromosome 4 containing the *CAMK2D* gene locus (Figure 4A). Compartments were relatively stable across this region in iPSCs and CMs, however the *CAMK2D* gene itself was located in a dynamic compartment that switched from inactive in iPSCs to active in CMs. Correspondingly, this gene was highly upregulated during differentiation to CMs (Figure 4A, inset).

We observed this effect on a global level, as genes located in A compartments were expressed at significantly higher levels than genes located in the B compartments in both iPSCs and CMs (Figure 4B). Additionally, genes that switched A/B compartments between cell types were correspondingly up- or down-regulated (Figure 4C). GO analysis of the 1,008 genes that switched from B to A compartments during iPSC-CM differentiation revealed enrichment for terms such as “cardiovascular system development” and “heart contraction” (Figure 4D, Supplementary File 5). Importantly, these genes were identified based solely on their location in a dynamic genomic compartment and not from gene expression data. GO analysis for genes that switched from A to B compartments during iPSC-CM differentiation related to non-cardiac processes, such as skin development, epithelial cell differentiation and sex determination (Figure 4—figure supplement 3, Supplementary Files 5 and 6). These data show that PCHi-C accurately captured tissue-specific interactions and indicate that compartmentalization of genes in spatially regulated regions of the nucleus may be one mechanism to ensure tissue-specific gene expression (Dixon et al. 2015). In summary, our analyses demonstrated that CM promoter interactions recapitulate key features of cardiac gene regulation and function, validating the CM map as an important tool to investigate CVD genetics.

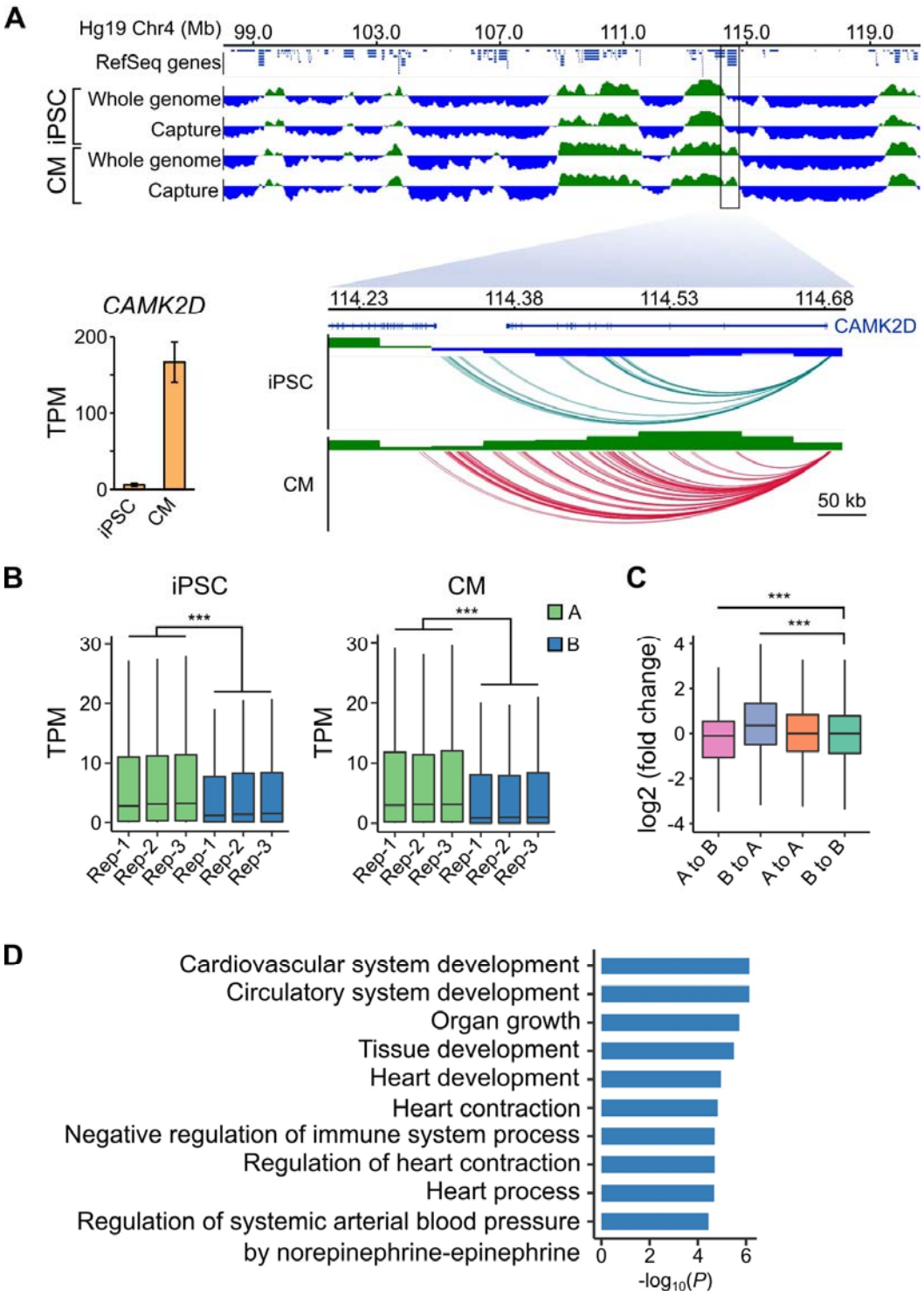

Figure 4. **A/B compartment switching corresponds to activation of tissue-specific genes. (A)** Top panel: 10 Mb region on chromosome 4 showing A (green) and B (blue) compartments based on the first principle component analysis calculated by HOMER (Heinz et al. 2010) of the whole-genome Hi-C and capture Hi-C interaction data. Bottom panel: zoomed in on the *CAMK2D* locus; only capture Hi-C A/B

compartments shown. Inset: expression level of *CAMK2D* in iPSCs and CMs across the three replicates. **(B)** Expression level (TPM) of genes located in the A (green) or B (blue) compartment in each replicate of iPSC (left) or CM (right). **(C)** Difference in expression level (log2 fold change relative to iPSCs) of genes switching compartments from iPSC to CM or remaining in stable compartments. **(D)** Gene Ontology analysis of biological processes associated with genes switching from B to A compartments during iPSC-CM differentiation. *** $P < 2.2x10^{-16}$, Wilcoxon rank-sum test.

CM promoter interactions link GWAS SNPs to target genes

A particularly relevant application of high resolution promoter interaction maps is to guide post-GWAS studies by identifying the target genes of disease-associated variants. We employed this approach to link GWAS SNPs for several major cardiovascular diseases to their target gene(s) using the CM interaction map. We compiled 524 lead SNPs from the NHGRI database (https://www.ebi.ac.uk/gwas/) for three important classes of CVDs: cardiac arrhythmias, heart failure, and myocardial infarction (Table 1, Supplementary Files 7 and 8). Because of linkage disequilibrium (LD) patterns, the true causal SNP could be any SNP in high LD with the lead variant. Therefore, we expanded this set of SNPs to include all variants in high LD ($r^2 > 0.9$, within 50 kb of lead SNP), increasing the number of putatively causal variants to 10,475 (hereafter called LD SNPs). We found that 1,999 (19%) of the LD SNPs were located in promoter-distal MboI fragments that interacted with the promoters of 347 genes in CMs (Supplementary File 8), hereafter referred to as target genes. The majority (89%) of LD SNP-target gene pairs were located within the same TAD, with a median distance of 185kb between each SNP-target gene pair (Figure 5A). Importantly, 90.4% of SNP-target gene interactions skipped at least one gene promoter and 42% of SNPs interacted with at least two different promoters (Figure 5B).

Table1. Summary of the SNPs and target genes characterized in each disease class

	Arrhythmia	Myocardial Infarction	Heart Failure	Combined
Number of studies	30	11	11	50
Tag SNPs	358	86	80	524
SNPs in LD	6,555	1,822	2,098	10,475
SNPs looping to genes	1,152	357	490	1,999
Target genes	237	72	53	347

Summary values for each disease group are depicted along with the total number of GWAS, SNPs, and target genes ("Combined" column). Tag SNPs were identified from the published GWAS in the NHGRI-EBI database; SNPs in LD are the total number of non-promoter SNPs (including tag SNPs) in LD (r^2 >0.9) with the tag SNPs in each disease group; SNPs looping to genes are the SNPs in LD that are in a distal promoter interaction; Target genes are all genes with an interaction to a promoter-distal SNP. See Supplementary File 8 for a complete list of all GWAS, coordinates of each SNP and its assigned target gene, expression level in iPSC and CM, and mouse knock-out phenotype where available.

To confirm that the CM PCHi-C interactions linked SNPs to CVD-relevant target genes, we performed GO analysis and found that target genes were highly and specifically enriched for biological processes related to cardiac function, such as membrane repolarization and cardiac conduction (Figure 5C, left panel and Supplementary Files 5 and 6). As a control, we used iPSC interactions to link the same SNPs to target genes and observed a completely different set of unrelated biological processes for these genes (Figure 5C, right panel). To further characterize the biological relevance of target genes, we mined mouse knock-out data from the Mouse Genome Informatics (MGI) database (Blake et al. 2017), which revealed that a statistically significant number of target genes resulted in a cardiovascular phenotype when knocked-out in the mouse (78 genes (22.4%), $P = 1x10^{-5}$, Figure 5D). Finally, we examined expression quantitative trait loci (eQTL) data from human left ventricle (LV) tissue and found that of the 1,999 LD SNPs in interactions, 410 (20.5%) corresponded to LV eQTLs; in comparison, only 12.2% of the full set of LD SNPs corresponded to LV eQTLs ($P < 0.00001$, Figure

5E). We next assessed whether eQTLs loop to their associated gene. For this analysis, we considered the full set of LV eQTLs, as the 410 LD SNP eQTLs represent too small of a proportion of the full set (<0.1% of all LV eQTLs) to fully ascertain significance. On a genome-wide level, LV eQTLs in promoter-distal interactions were significantly more likely to loop to their associated gene than expected by chance ($P < 0.00001$, Figure 5F, left panel). Importantly, this significance decreased when LV eQTLs were analyzed with iPSC promoter interactions ($P = 0.035$, Figure 5F, right panel). Taken together, these results indicate that CM promoter interactions identify a subset of disease-relevant SNPs most likely to be functional and support the use of the CM map to assign distal CVD-associated SNPs to putative target genes.

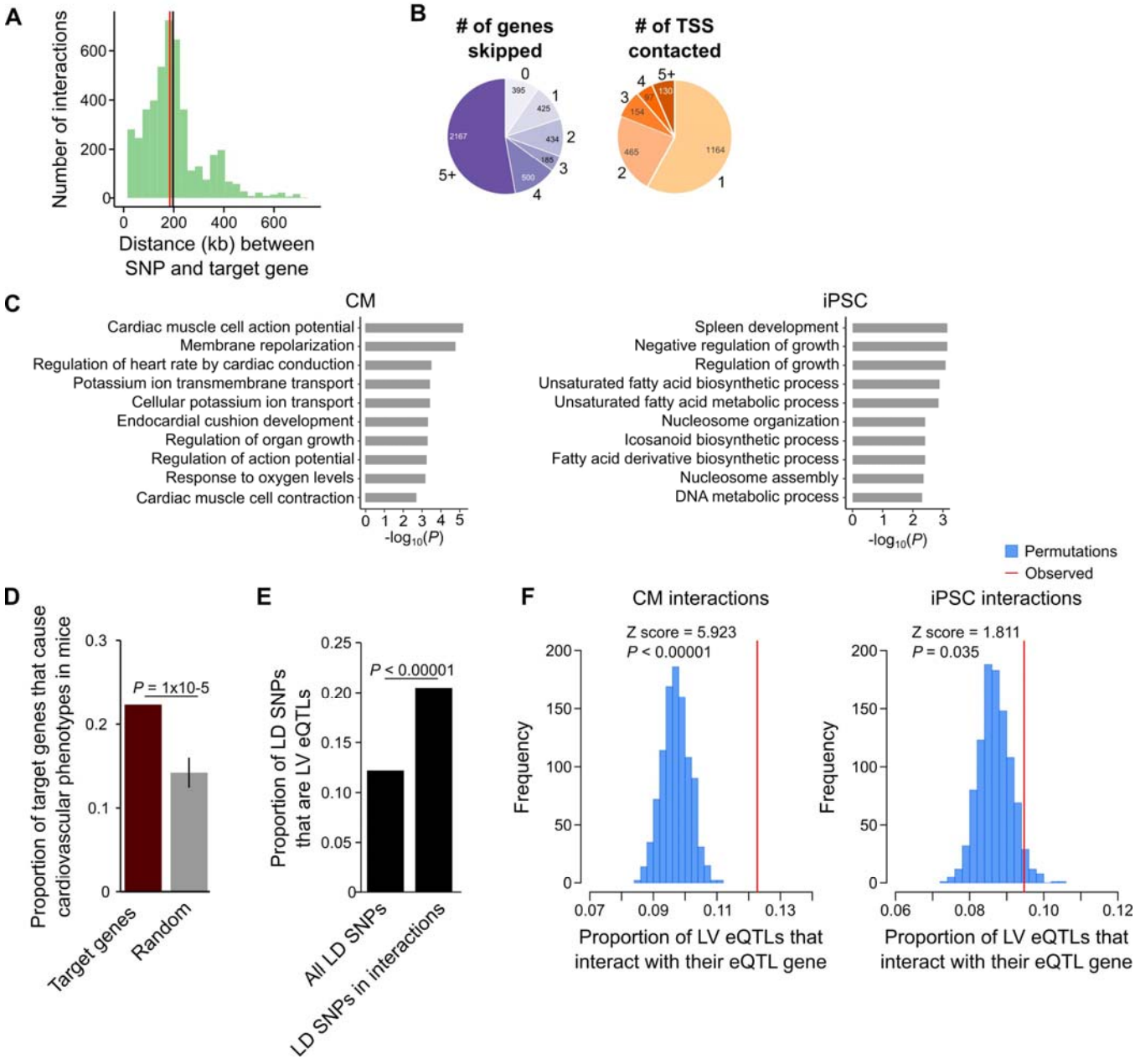

Figure 5. CM promoter interactions link CVD GWAS SNPs to target genes. (A) Distribution of genomic distances separating SNP-target gene interactions (red line, median = 185 kb; black line, mean = 197 kb). **(B)** Pie chart showing the number of TSS's skipped for each SNP-target gene interaction (left) and the number of genes contacted by each SNP (right). **(C)** GO enrichment analysis for genes looping to LD SNPs using the CM promoter interaction data (left panel) or the iPSC promoter interaction data (right panel). **(D)** Proportion of target genes that result in a cardiovascular phenotype when knocked-out in the mouse (MGI database (Blake et al. 2017)), compared to a random control set.

P-value calculated with a Z-test. **(E)** Proportion of GWAS LD SNPs that are eQTLs in left ventricle (LV) when considering either the full set of LD SNPs, or the subset that overlap CM promoter interactions. P-value calculated with Fisher's exact test. **(F)** Proportion of LV eQTLs (genome-wide) that map within a promoter interaction for the eQTL-associated gene (indicated by the red line). Random permutations were obtained by re-assigning each promoter's set of interactions to a new promoter and calculating the proportion of eQTLs in random interactions that interact with their eQTL-associated gene. Proportions only consider eQTLs that overlap a promoter-distal interaction. P-values calculated with a Z-test.

Using gene expression as a metric for interpreting disease-relevance of newly identified target genes

Based on an enrichment of target genes with known cardiac function, we next assessed whether expression level is an informative metric to further prioritize functional follow-up studies. We examined the expression level of the 347 target genes and found that they were moderately over-expressed in CMs compared to iPSCs (median log2 fold change = 1.08, mean log2 fold change = 1.44, mean TPM values were 40.6 in iPSCs and 60.1 in CMs, P = 0.12, Figures 6A and 6B). Although not significant, this result reflects the enrichment of known cardiac-related genes that interact with CVD loci. However, because a subset of target genes was over-expressed in iPSCs relative to CMs (Figure 6C), we predicted that gene expression level alone may be an insufficient metric to gauge the relevance of target genes to CVD biology. Indeed, we found that 21 of the 78 target genes (27%) that cause cardiovascular phenotypes when knocked-out in mice were overexpressed in iPSCs compared to CMs (Supplementary File 8). This result indicates that putatively causal genes may not appear as obvious candidates based solely on gene expression data.

To illustrate this point, we highlight two genes: *TBX5*, a gene directly linked to cardiac arrhythmia (Figure 6D) (Smemo et al. 2012; Arnolds et al. 2012), and *LITAF*, a gene that, until recently, had no obvious role in cardiac biology (Moshal et al. 2017) (Figure 6E). Both genes formed long-range interactions to LD SNPs identified in arrhythmia GWAS, making both genes candidate functional targets of the GWAS associations. *TBX5*, which is over-expressed in CMs (Figure 6C), is the most likely target

449 gene of the LD SNPs nearby based on the interaction data but also because of its known role in
450 directing proper development of the cardiac conduction system. *LITAF*, on the other hand, was over-
451 expressed in iPSCs compared to CMs (Figure 6C), and was not known to contribute to cardiac function
452 until a recent study identified this gene as a regulator of cardiac excitation in zebrafish hearts (Moshal
453 et al. 2017).

454

455

456

457

458

459

460

461

462

463

464

465

466

467

468

469

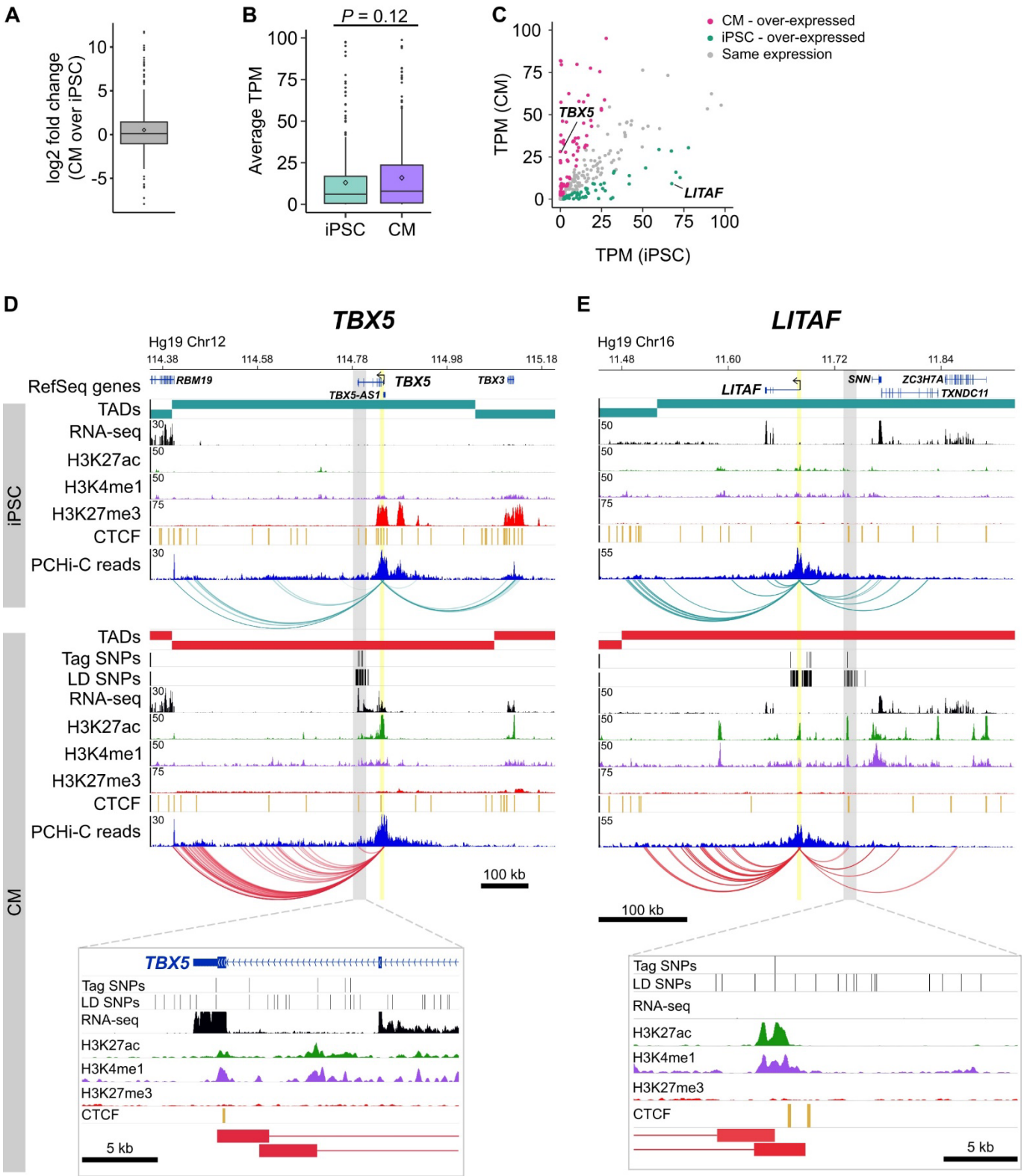

Figure 6. Characterizing target genes based on expression level. (A) Log2 fold change of the expression level of target genes in CMs compared to iPSCs (horizontal bar indicates median, 1.08; diamond indicates mean, 1.44). **(B)** Average TPM values of target genes in iPSCs and CMs (P = 0.12, Wilcoxon rank-sum test). Diamonds indicate the mean value (40.6 for iPSC, 60.1 for CM). **(C)** Comparison of average TPM values for target genes in CMs and iPSCs. See Supplementary File 8 for full list of genes and TPM values. **(D,E)** Examples of genes looping to cardiac arrhythmia GWAS SNPs in CMs. **(D)** The *TBX5* gene interacts with a functionally validated arrhythmia locus (Smemo et al. 2012). **(E)** The *LITAF* gene interacts with a locus identified in (Arking et al. 2014). Yellow highlighted region indicates the promoter; gray box and zoom panel show the promoter-interacting regions overlapping arrhythmia SNPs. For clarity, only interactions for the indicated promoter are shown.

CM promoter interactions are informative to cardiovascular associations that do not directly involve cardiomyocytes

Because the three disease classes that we analyzed represent diverse pathologies, we predicted that the target genes identified for each class individually may relate to different biological processes. Specifically, we considered that cardiac arrhythmias – which directly result from defects in cardiomyocytes specialized for electrical conduction – may uncover the most cardiac-relevant target genes compared to heart failure and myocardial infarction, two CVDs that also involve non-cardiac systems. When broken down into the respective disease classes, we confirmed that the majority of the GO enrichment for cardiac terms was driven by the cardiac arrhythmia SNPs (Figure 7A), with terms directly related to the cardiac conduction system. Myocardial infarction (Figure 7B) and heart failure (Figure 7C) analyses uncovered a set of genes that were slightly enriched for regulation of growth and morphogenesis, respectively.

Despite these seemingly non-specific processes, each set of target genes contained important disease-relevant candidates. For example, one of the strongest associations for myocardial infarction lies in-between the *CELSR2* and *PSRC1* genes on chromosome 1p13, but a careful screen of genes whose expression was affected by the risk allele implicated the more distal *SORT1* gene (Musunuru et al. 2010). *SORT1* encodes a sorting receptor that is expressed in many tissues and has been shown to act in the liver to regulate cholesterol levels (Petersen et al. 1997; Musunuru et al. 2010). Despite

functioning in the liver, we identified multiple promoter interactions between *SORT1* and the myocardial infarction GWAS locus in CMs (Figure 7D), directly implicating *SORT1* as the target gene and lending further support to experimental validation of this locus as a *SORT1* enhancer (Musunuru et al. 2010). Additionally, the *ACTA2* gene is located 220 kb away from the heart failure GWAS locus proximal to the *CH25H* and *LIPA* genes on chromosome 10q21 (Smith et al. 2010) (Figure 7E). *ACTA2* encodes the smooth muscle cell-specific actin protein and mutations in this gene have been shown to cause coronary artery disease, among other vascular diseases (Guo et al. 2009). Despite its location at a considerable distance from the GWAS association, chromatin interactions provide an important level of evidence that *ACTA2* is a putative causal gene in the development of heart failure. Therefore, the CM interaction map is not only useful to interrogate diseases directly related to cardiomyocytes, as in the case of cardiac arrhythmias, but also aids interpretation of target genes that may act in non-cardiac tissues.

523

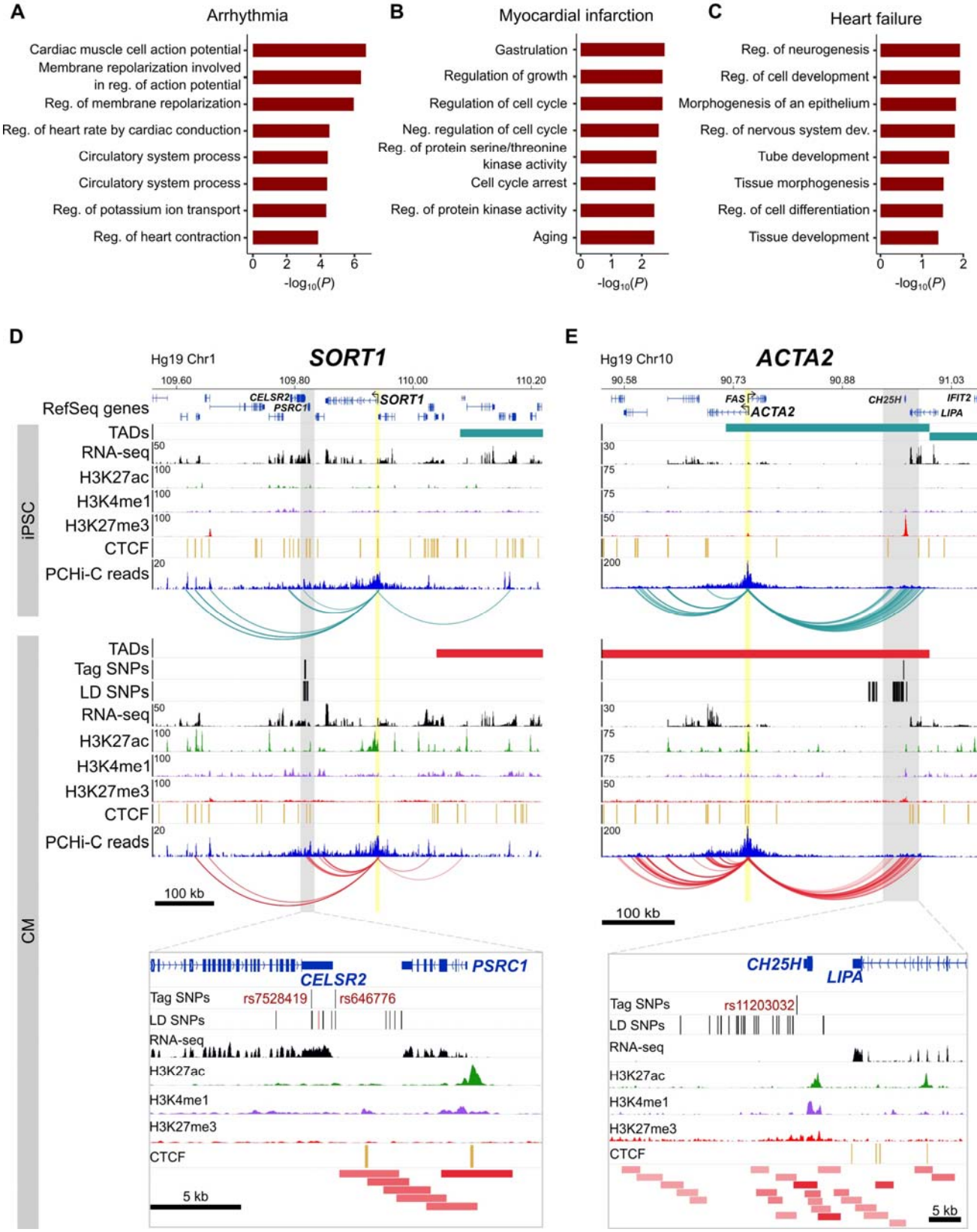

524

Figure 7. Relevance of CM promoter interactions for cardiac arrhythmia, myocardial infarction and heart failure. (A-C) Gene Ontology analysis for target genes looping to **(A)** cardiac arrhythmia SNPs, **(B)** myocardial infarction SNPs, and **(C)** heart failure SNPs. **(D)** The *SORT1* promoter loops to a distal myocardial infarction locus (Musunuru et al. 2010). The rs12740374 SNP shown to disrupt a C/EBP binding site in (Musunuru et al. 2010) is colored red. **(E)** The *ACTA2* promoter loops to the 10q21 heart failure locus (Smith et al. 2010). Zoom plots depict the full interacting region overlapping GWAS LD SNPs. For clarity, only interactions for the indicated gene are shown.

Discussion

Incomplete understanding of long-range gene regulation is a major roadblock in the translation of GWAS-associated loci to disease biology. Major challenges in this process include identifying putatively causal variants mapping within regulatory elements and functionally connecting these regulatory elements to their target genes. To delineate gene-regulatory interactions between CVD-associated SNPs and putative causal genes, we generated high-resolution maps of promoter interactions in human iPSCs and iPSC-derived CMs. We demonstrated that promoters interact with a diverse set of distal DNA elements in both cell types, including known enhancer sequences, which reflect cell identity and correspond to tissue-specific gene expression. To demonstrate the utility of the CM map, we linked 1,999 CVD-associated SNPs to putative causal target genes which identified both validated and potentially novel genes important for cardiovascular disease biology. To validate the biological relevance of our maps, we addressed several important features of long-range chromatin interactions in comparative analyses.

Promoters contact distal regions enriched for tissue-specific transcription factor motifs

Gene regulation by distant regulatory elements involves the bridging of linearly separated DNA sequences, for example between a promoter and its distal enhancers, through chromatin looping mechanisms (Spitz and Furlong 2012). In support of this model, we report an enrichment of tissue-defining transcription factor motifs in the distally interacting sequences of differentially expressed promoters both for CMs and iPSCs, providing an important level of evidence to validate the functional

552 relevance of iPSC and CM interactions. One explanation for this enrichment is that our interaction maps
553 are high resolution. We generated Hi-C libraries with the 4-bp cutter MboI, which generates fragments
554 with an average size of 422 bp; this increased specificity of the captured region likely leads to better
555 resolution of the underlying enhancer sequence and, consequently, increased power to detect short
556 transcription factor binding motifs.

557 *Influence of active and repressive promoter interactions on gene expression level*

558 The majority of capture Hi-C studies to date have reported that gene expression level correlates
559 with enrichment for various histone marks. We observed the same trend in our data, with highly
560 expressed genes exhibiting strong enrichment for looping to distal H3K4me1 and H3K27ac-marked
561 regions, and lowly expressed genes exhibiting strong enrichment for looping to H3K27me3-marked
562 regions. These data are consistent with a model in which the number of long-range interactions to
563 enhancers or repressors additively contributes to gene expression level (Schoenfelder et al. 2015;
564 Javierre et al. 2016). The forces that drive increased association between promoters and distal *cis*-
565 regulatory elements are not completely understood and have been topics of investigation in the
566 genome organization and chromatin biology fields for several years (Dekker and Mirny 2016; Calo and
567 Wysocka 2013). One possibility is that this increasing enrichment is driven by genomic
568 compartmentalization of active and inactive chromatin. We showed that a gene's expression level
569 correlates with the number of histone ChIP-seq peaks within a large window (300 kb) surrounding each
570 promoter. Thus, highly expressed genes are more likely to contact active chromatin regions compared
571 to lowly expressed genes, corresponding to the observed increasing enrichment we and others have
572 reported. This local increase in active or repressive chromatin may be one driving force underlying the
573 expression level-dependent increase in association between promoters and *cis*-regulatory elements,
574 akin to a phase separation-mediated model of enhancer-promoter interactions (Hnisz et al. 2017).

575 *A promoter interaction map for cardiovascular disease genetics*

We demonstrated several ways in which promoter interaction data can be used to better understand disease genetics, specifically addressing the major requirement for a high-resolution map of the gene-regulatory network in human cardiomyocytes. Although iPSC-derived CMs are known to be relatively immature and do not fully reflect the diverse structural and functional aspects of adult cardiac cells (Gherghiceanu et al. 2011; Karakikes et al. 2015), the difficulty in obtaining pure sub-populations of primary cardiomyocytes with high integrity necessitates the use of an *in vitro* system. We showed that the CMs used in this study were highly pure and recapitulate known gene regulatory properties of primary cardiomyocytes. Because of this purity, we were able to integrate CVD-associated SNPs with CM promoter interactions with high confidence, assigning nearly 20% of the variants in high LD with these associations to 347 target genes.

Supporting the physiological relevance of CMs to the cardiac conduction system, we found that target genes were most relevant for GWAS loci associated with cardiac arrhythmias, in line with previous findings in immune cells that many target gene interactions were unique to relevant immune cell subtypes (Javierre et al. 2016; Mumbach et al. 2017). Our data also revealed that even for diseases whose etiology involves cell types other than cardiomyocytes, such as myocardial infarction and heart failure, we identified interactions involving loci associated with these diseases that recapitulate the enhancer-promoter interactions in non-cardiac cell types. As an example, we showed that a validated myocardial infarction locus interacts with the distal *SORT1* promoter in CMs even though this locus has been extensively characterized in the context of cholesterol metabolism in hepatocytes. Therefore, the promoter interactions we observe linking the disease locus to *SORT1* may represent tissue-invariant genome architecture, likely reflecting that genome organization in general is relatively stable (Dixon et al. 2015; Jin et al. 2013; Ghavi-Helm et al. 2014). While we advocate the use of the CM map for investigating gene regulatory mechanisms of diseases related to cardiomyocyte biology, we also emphasize that, where identified, any interaction between a promoter and a putative

disease-associated genomic region serves as an important level of evidence to prioritize that gene for future follow-up studies.

Limitations of the PCHi-C maps

The PCHi-C technique holds great promise to identify with high resolution and throughput all regulatory elements for all genes in any tissue or developmental stage of interest. However, due to technical and biological limitations, there are important caveats to PCHi-C that should be considered when interpreting the iPSC or CM interaction data. The most important caveat is that there are likely to be many false negatives, or “missing” interactions. Although the capture step greatly enriches for promoter-containing ligation fragments in a Hi-C library, the total landscape of promoter contacts in a population of cells is still under-sampled, even with a sequencing depth of ~400M reads per replicate conducted for this study. This is due to several factors, including the hybridization efficiency of each bait, ability to design sufficient baits per promoter, and the transient nature of many regulatory interactions. This latter issue is confounded by the distance-dependent effect on ligation frequency: as the distance between two fragments increases, the read-depth required to robustly identify that interaction also increases. Because many regulatory elements are located far from their target gene(s), very deep sequencing is required to identify them with high confidence. The feasibility of deeper sequencing and modifications to computational pipelines will continue to improve the coverage and resolution of Hi-C data. Nevertheless, the data sets we provide here represent a highly enriched set of ~350,000 and ~400,000 promoter interactions in iPSC and CMs, respectively; although there are likely missing interactions, the interactions that we did identify should be considered as very high confidence, as they were independently identified in at least two biological replicates and show strong signal of enrichment for known features of genome architecture and gene regulation.

In conclusion, the promoter interaction maps we generated in this study represent important resources for any investigation into the gene regulatory mechanisms underlying cardiovascular disease traits. The list of candidate regulatory variants and their target genes may serve as an entry point for

625 several hypotheses related to CVD GWAS, and can be readily tested in experimental settings. To
626 provide both the iPSC and CM maps as an accessible resource, we have hosted the full set of data
627 presented in this study at the WashU EpiGenome Browser. Additionally, we provide the significant
628 PCHi-C interaction files used in all analyses in the Supplementary Material (Supplementary Files 1 and
629 2); these can be applied to future multi-omics analyses of gene regulation and disease genetics.

630

631 **Methods**

632 ***Tissue culture of iPSCs***

633 We used the Yoruban iPSC line 19101, kindly provided by the laboratory of Yoav Gilad. This
634 iPSC line was reprogrammed from lymphoblastoid cells as part of a previous study, where it was shown
635 to differentiate into all three germ layers, displayed a normal karyotype, and expressed markers
636 characteristic of pluripotency (Banovich et al. 2018). iPSCs were grown in Essential 8 (E8) Medium
637 (Thermo Fisher #A1517001) supplemented with 1X Penicillin-Streptomycin (Pen/Strep, Gibco) on
638 Matrigel-coated tissue culture dishes (Corning #354277). Cells were passaged when they were ~80%
639 confluent using enzyme-free dissociation solution (30mM NaCl, 0.5mM EDTA, 1X PBS minus
640 Magnesium and Calcium) and maintained in E8 Medium with 10μM Y-27632 dihydrochloride (Abcam
641 #ab120129) for 24 hours. Medium was replaced daily. iPSC cultures routinely tested negative for
642 mycoplasma contamination using the Universal Mycoplasma Detection Kit (ATCC #30-1012K).

643 ***Cardiomyocyte differentiation***

644 Cardiomyocyte differentiations were based on the protocol of Burridge *et al.* (Burridge et al.
645 2014) with modifications described in Banovich *et al.* (Banovich et al. 2018). iPSCs were expanded in
646 60 mm dishes in E8 media until they reached 60-70% confluency at which time the differentiation was
647 started (day 0). On day 0, E8 media was replaced with 10mL of basic heart media/12μM GSK-3
648 inhibitor CHIR-99021 trihydrochloride (Tocris #4953)/Matrigel overlay [basic heart media: RPMI 1640

minus L-glutamine (HyClone #SH30096.01) with 1X GlutaMax (Life Technologies #11879020) supplemented with 1X B27 minus insulin (Thermo Fisher #A1895601) and 1X Pen/Strep; Matrigel overlay was accomplished by dissolving Matrigel in 50mL basic heart media at a concentration of 0.5X according to the lot-specific dilution factor]. After 24 hours (day 1), the GSK-3 inhibitor was removed by replacing media with 10 mL basic heart media. On day 3, media was replaced with 10 mL basic heart media supplemented with 2 µM Wnt-C59 (Tocris #5148). On day 5 (48 hours later), media was replaced with 10 mL basic heart media. On day 7, cells were washed once with 1X PBS and then 15 mL basic heart media was added. Media was replaced every other day in this way until day 15 at which time cardiomyocytes were selected for by replacing basic heart media with 10mL lactate media (RPMI 1640 minus D-glucose, plus L-glutamine (Life Technologies #11879020), supplemented with 0.5 mg/mL recombinant human albumin (Sigma 70024-90-7), 5 mM sodium DL-lactate (Sigma 72-17-3), 213 µg/mL L-ascorbic acid 2-phosphate (Sigma 70024-90-7) and 1X Pen/Strep). Lactate media was replaced every other day until day 20 at which point cardiomyocytes were harvested. Cells from successful differentiations exhibited spontaneous beating around days 7-10.

Cardiomyocytes were harvested by washing once with 1X PBS followed by incubation in 4 mL TrypLE (Life Technologies 12604-021) at 37°C for 5 minutes. After incubation, 4 mL lactate media was added to the TrypLE and a 1 mL pipet was used to dislodge cells. Cells were strained once with a 100µM strainer and then once with a 40µM strainer. Cells were pelleted at 500xg and then resuspended in PBS and counted. For each batch of differentiation, 5 million cells were taken for promoter-capture Hi-C and 1 million cells were taken for RNA-seq. To assess purity, 2 million cells were taken for flow cytometry analysis using an antibody for cardiac Troponin T (BD Biosciences 564767). All cells used in downstream experiments were at least 86% Troponin T positive (Figure 1—figure supplement 1A). We carried out three independent differentiations of the same iPSC line and generated promoter-capture Hi-C and RNA-seq libraries in iPSCs and CMs from each triplicate.

Promoter capture Hi-C

-Crosslinking cells

iPSCs or cardiomyocytes were harvested from tissue culture dishes and counted. Cells were resuspended in 1X PBS at a concentration of 1 million cells/mL and 37% formaldehyde was added to a final concentration of 1%. Crosslinking was carried out for 10 minutes at room temperature on a rocking platform. Glycine was added to a final concentration of 0.2 M to quench the reaction. The cells were pelleted, snap frozen in liquid nitrogen and stored at -80°C until ready for Hi-C processing.

-in situ Hi-C

We prepared all promoter capture Hi-C libraries in one batch using three crosslinked pellets of 5 million cells for both iPSCs and iPSC-derived cardiomyocytes, representing three independent cardiomyocyte differentiations. The *in situ* Hi-C step was performed as in Rao *et al.* (Rao et al. 2014) with a single modification in which NEBNext reagents from the NEBNext Multiplex Oligos for Illumina kit were used (NEB #E7335S) instead of Illumina adapters, following the manufacturer's instructions. Hi-C libraries were amplified directly off of T1 beads (Life Technologies #65602) using NEBNext primers and 6 cycles of PCR.

-Promoter capture – probe design and generation

Hi-C capture probes were designed to target four MboI restriction fragment ends (120 bp) near the TSS of protein coding RefSeq genes (O'Leary et al. 2016) mapped to hg19 in the UCSC Genome Browser (Speir et al. 2016). To select restriction fragments, we only kept MboI restriction fragments longer than 200 bp and overlapping 10 kb around a RefSeq TSS. TSSs closer than 1 kb from each other were excluded, as their interactions were likely to be captured by the other RefSeq TSS. The four MboI restriction fragments ends closest to each RefSeq TSS were selected as putative probes. The 120 bp sequences were submitted to Agilent's SureDesign proprietary software for probe selection, which can slightly shift the location and remove probes. In total, we ordered a library of 77,476 single-stranded DNA oligos from CustomArray, Inc. (www.customarrayinc.com). Each oligo consisted of the

sequence 5'-ATCGCACCAGCGTGTN$_{120}$CACTGCGGCTCCTCA-3' (Gnirke et al. 2009) where N$_{120}$ represents the 120 nucleotides adjacent to the MboI cut site. The complete list of oligo probes and their corresponding gene name is provided in Supplementary File 9.1.

The oligos arrived as a pool containing 1000 ng of material. We used 16 ng of the oligo pool in a PCR reaction to make them double stranded using primers 5′-CTGGGAATCGCACCAGCGTGT-3′ (Primer A), and 5′-CGTGGATGAGGAGCCGCAGTG-3′ (Primer B) as in (Gnirke et al. 2009). The PCR reaction was cleaned using AMPure XP beads (Agencourt #A6388) and eluted with 20µl of water. To add the full T7 promoter to the 5' end of the oligos, a second PCR reaction was carried out using 10ng of the cleaned-up first-round PCR product with the forward primer 5'-GGATTCTAATACGACTCACTATAGGGATCGCACCAGCGTGT-3' (Primer A T7). We purified the PCR product corresponding to 176 bp using a Qiagen gel extraction kit (#28704). To generate biotinylated RNA baits, we performed *in vitro* transcription on the double-stranded library using the MEGAshortscript T7 Transcription Kit (Thermo Fisher #AM135) with Biotin-16-dUTP (Sigma #11388908910). After DNase treatment the transcription reaction was cleaned using the MEGAclear kit (Thermo Fisher #AM1908) and eluted with 50µl elution buffer. We confirmed the correct bait size on a denaturing gel.

-Promoter capture – hybridization with Hi-C library

To isolate promoter-containing fragments from the whole-genome *in situ* Hi-C library, we hybridized the biotinylated RNA bait pool with the Hi-C library as follows. A mix containing 500ng of the Hi-C library, 2.5µg of human Cot-1 DNA (Invitrogen #15279-011), 2.5µg of salmon sperm DNA (Invitrogen #15632-011), 0.5µl blocking primer P5 (IDT #1016184), and 0.5µl blocking primer P7 (IDT #1016186) was heated for 5 min. at 95°, held at 65° and mixed with 13µl pre-warmed hybridization buffer (10X SSPE, 10X Denhardt's, 10 mM EDTA and 0.2% SDS) and a 6 µl pre-warmed mix of 500ng of the biotinylated RNA bait and 20U SUPERase-In (Thermo Fisher #AM2694). The hybridization mix

was incubated for 24h at 65°C. To isolate captured fragments, we prepared 500ng of streptavidin-coated magnetic beads (Dynabeads MyOne Streptavidin T1, Thermo Fisher #65601) in 200µl of Binding buffer (1M NaCl, 10mM Tris-HCl pH 7.5, 1mM EDTA). The hybridization mix was added to the Streptavidin beads and rotated for 30 minutes at room temperature. The beads containing the captured Hi-C fragments were washed with 1X SSC, 0.1% SDS for 15 minutes at room temperature, followed by three washes (10 min each) at 65°C with 0.1X SSC/0.1% SDS. After the final wash, the beads were resuspended in 22µl of water and proceeded to post-capture PCR. The PCR reaction was performed with 11µl of the “capture Hi-C beads” and 8 cycles of amplification. An AMPure XP bead purification was used to clean the PCR reaction and DNA was quantified using the QuantiFluor dsDNA System (Promega #E2670) and a High Sensitivity Bioanalyzer. Final capture Hi-C libraries were subjected to 100bp paired-end sequencing on an Illumina HiSeq 4000 machine. Read count summaries are provided in Supplementary File 9.2.

Interaction calling

We used HiCUP v0.5.9 (Wingett et al. 2015) to align and filter Hi-C reads (total and filtered read counts are presented in Supplementary File 9.2). Unique reads were given to CHiCAGO version 1.2.0 (Cairns et al. 2016) and significant interactions were called with default parameters. In this study, we focused exclusively on *cis*-interactions as the evidence that *trans*-chromosomal interactions contribute to gene expression regulation is limited. CHiCAGO reports interactions for each captured restriction fragment; to summarize interactions by gene, we considered the interval spanning all captured MboI fragments (i.e. the set of probes spanning each TSS) as the promoter region ("merged TSS"). This means the promoter regions created have variable lengths. In cases where multiple genes were annotated to the same promoter region, we report the interaction for each gene individually. This annotation allowed us to perform gene-level analyses, for example based on expression level. We removed this redundancy as necessary, for example in motif enrichment analyses of the promoter-interacting fragments. Using the "merged TSS" interaction files, we filtered interactions to retain those

that mapped within 1kb of each other in at least two replicates. Specifically, we extended each promoter-interacting fragment by 1kb on each end and then used BEDTools (Quinlan and Hall 2010) pairToPair functionality to identify interactions where both ends matched across replicates. To identify cell type-specific interactions, we required that the interaction (with the 1 kb extension) was not present in any of the three replicates of the other cell type. The number of read-pairs per promoter and the corresponding number of significant interactions identified is presented in Supplementary File 9.3. The TAD analyses, motif enrichment, ChIP-seq peak enrichment, and eQTL analyses (related to Figures 1, 2, 3 and 5) were conducted with fragment-level interactions (no 1kb extension). The GWAS SNP analyses were conducted with 1kb-extended interactions, as we aimed to be as inclusive as possible when linking CVD SNPs to target genes.

4C-style plots

To generate the by-gene read counts displayed in the genome-browser figures, all read-pairs mapping to captured MboI fragments for a given promoter were summed across replicates. Specifically, we summed reads for each MboI fragment where the read was part of a paired-read that mapped to a bait for the given gene. The arcs that are displayed underneath the 4C-style plot represent significant interactions that were identified in at least two replicates as detailed above in “Interaction calling”.

TAD analysis

To identify TADs, we pooled reads across replicates for each cell type using the pre-capture Hi-C data (600M reads for iPSC and 733M reads for CM) and used HiCUP v0.5.9 (Wingett et al. 2015) to align and filter Hi-C reads. HOMER v4.8.3 (Heinz et al. 2010) was used to generate normalized interaction matrices at a resolution of 40 kb and then TopDom v0.0.2 (Shin et al. 2016) was used with a window size w=10 to identify topological domains, boundaries and gaps. We only considered domains for the analyses in this paper. We considered a promoter capture Hi-C interaction to be “intra-TAD” if

770 the entire span of the interaction was fully contained in a single domain. “Inter-TAD” interactions are
771 defined as interactions where each end maps to a different domain.

772 ***A/B compartments***

773 The program runHiCpca.pl from the HOMER (Heinz et al. 2010) v4.8.3 package was used to
774 call A/B compartments with -res 50000 for both whole-genome and capture Hi-C data.

775 ***RNA-seq***

776 Total RNA was extracted from flash-frozen pellets of 1 million cells using TRI Reagent (Sigma
777 #T9424) and a homogenizer followed by RNA isolation and clean-up using the Direct-zol RNA Kit
778 (Zymo Research #11-331). RNA-seq libraries were generated with the Illumina TruSeq V2 kit (Illumina,
779 RS-122-2001) and 1µg of RNA, following manufacturer’s instructions. Libraries were made from RNA
780 isolated from three independent iPSC-CM differentiations (triplicates of iPSC and of cardiomyocytes).
781 Libraries were sequenced on an Illumina HiSeq 4000.

782 Gene counts were quantified with Salmon 0.7.2 (Patro et al. 2017) and imported with tximport
783 1.2.0 (Soneson et al. 2015) into DESeq2 1.12.4 (Love et al. 2014) to call differentially expressed genes.
784 A minimum 1.5-fold-difference between CMs and iPSC triplicates and a minimum adjusted P-value of
785 0.05 were required to select differentially expressed genes for downstream analyses. TPMs (transcripts
786 per million) were also estimated by Salmon. Because the samples clearly clustered according to their
787 known tissues of origin (Figure 1 – figure supplement 2A), no correction for batch effects was
788 performed.

789 ***H3K27ac ChIP-seq for comparison with Epigenome Roadmap samples***

790 We performed ChIP-seq on 2.5 million cells each for iPSCs and CMs using H3K27ac antibodies
791 (Wako #306-34849). Briefly, cells were crosslinked with 1% formaldehyde for 10 minutes at room
792 temperature, quenched with 0.2M glycine for 5 minutes, pelleted and snap-frozen in liquid nitrogen.
793 Cells were lysed in Lysis Buffer 1 (50 mM HEPES-KOH, pH 7.5, 140 mM NaCl, 1 mM EDTA, 10%

glycerol, 0.5% NP-40, 0.25% Triton X-100). Crosslinked chromatin was sheared to an average size of 300 bp using a Bioruptor with 30" on/30" off at high setting and then incubated overnight at 4ºC with 1 µg antibody. Dynabeads M-280 Sheep Anti-Mouse IgG (ThermoFisher #11201D) were used to pull down chromatin and ChIP DNA was eluted and prepared for sequencing using the NEBNext Ultra II DNA Library prep kit (NEB #E7645S). ChIP-seq reads were aligned with Bowtie 2-2.2.3 (Langmead and Salzberg 2012) and peaks were called with HOMER (Heinz et al. 2010) v4.8.3 on unique reads with mapping quality > 10 using the –region and –style histone parameters. Significant peaks were overlapped with H3K27ac peaks from Epigenome Roadmap samples which demonstrated high concordance between matched tissue types (Figure 1—figure supplement 2C,D). Because we performed a low level of sequencing, we did not identify as many peaks as the Roadmap samples. Therefore we used Roadmap ChIP-seq data in all of our analyses.

Gene Ontology analysis

The human Gene Ontology (GO) associations of GO terms (Ashburner et al. 2000) to genes and the GO database were downloaded on January 22, 2016 from http://geneontology.org/gene-associations. GO terms were associated with RefSeq genes via gene symbols. Using the GO annotation graph, all parent terms were assigned to the terms annotated to a gene. A hypergeometric test was used to calculate the statistical significance of the difference of the number of genes associated with a given GO term in a particular gene set and the universe of all RefSeq genes ($P < 0.05$). P-values were corrected with the R package p.adjust function using the "fdr" method.

For two of the GWAS disease groups (heart failure and myocardial infarction), the list of genes looping to LD SNPs included many histone genes. This is because there is a tag SNP located in the middle of a histone gene cluster (containing > 30 histone genes located close together) in each case. After expanding the tag SNP to all SNPs in LD, many of the histone genes in that cluster looped to the LD SNPs, resulting in a high representation of these genes in the final gene list. The resulting Gene Ontology enrichment analysis gave terms relating to nucleosome and chromatin organization because

819 of this over-representation. We therefore chose to remove these genes from the final gene lists of heart
820 failure and myocardial infarction target genes.

821 ***Motif analysis***

822 The program findMotifsGenome.pl from the HOMER (Heinz et al. 2010) v4.8.3 package was
823 used with –size given parameter to identify overrepresented motifs in the distal (non-promoter)
824 interacting sequences of promoter interactions. As stated above, this analysis was performed on
825 fragment-level promoter-interacting sequences.

826 ***Histone ChIP-seq enrichment analysis***

827 We obtained publicly available ChIP-seq data in the form of processed peak calls for H3K27ac,
828 H3K4me1 and H3K27me3 from the Roadmap Epigenomics Project (Roadmap Epigenomics
829 Consortium et al. 2015), and for CTCF from ENCODE (ENCODE Project Consortium 2012)
830 (Supplementary File 10). We only considered peaks that mapped outside of the captured region of
831 promoters to ensure our results were not driven by the strong peak signal over most promoters. As a
832 proxy for iPSCs, we used data from the H1 embryonic stem cell line and for CMs we used data from
833 Left Ventricle tissue. We grouped genes into five expression categories based on the average TPM
834 values: group 1 (0 TPM), group 2 (TPM 0-3), group 3 (TPM 3-25), group 4 (TPM 25-150) and group 5
835 (TPM >150) and for each group of genes, we calculated the enrichment for promoter interactions to
836 overlap a given feature. To calculate enrichment of interactions overlapping an epigenetic feature, we
837 compared the observed proportion of MboI fragments in significant interactions overlapping a feature to
838 the proportion of random MboI fragments overlapping the feature. Specifically, we randomly selected
839 MboI fragments from a set that excluded fragments mapping within captured regions (promoters) or
840 within unmappable genomic regions (gaps). The number of randomly selected fragments matched the
841 number of interacting fragments considered for the analysis. We performed 100 iterations of
842 overlapping random fragments with a feature and report the average fold-enrichment. We refer to this

method of enrichment as a "genome-wide" background model because for each gene expression group, the observed proportion of fragments containing a peak is compared to randomly selected fragments from the whole genome.

To calculate the correlation between expression and histone ChIP-seq peak density, we calculated the Spearman's rank correlation between the expression value for each gene (the average TPM value) and the number of peaks mapping within 300 kb of each gene TSS. We only considered genes with at least one significant interaction in the respective cell type to allow for generalizations to the enrichment analysis presented in Figure 3.

GWAS analysis

We compiled genome-wide significant SNPs associated with GWAS for cardiac arrhythmia, heart failure, and myocardial infarction from the NHGRI-EBI database (http://www.ebi.ac.uk/gwas/); see Supplementary File 7 for list of terms used to identify specific GWAS. We expanded each set of SNPs to all SNPs in high LD ($r^2 > 0.9$) using phase 3 data of the 1,000 genomes project (Nikpay et al. 2015) (Supplementary File 3). For each lead SNP from the GWAS we analyzed, we selected a 100 kb interval centered on the SNP (SNP +/- 50kb). For each 100 kb interval, Tabix (Li 2011) was used to retrieve genotypes. We then used PLINK (Purcell et al. 2007) v1.90p on phase 3 data from the 1,000 genomes project (Nikpay et al. 2015) (ftp.1000genomes.ebi.ac.uk/vol1/ftp/release/20130502, v5a) to select SNPs in LD ($r^2 > 0.9$) with the tag SNP and a minimum allele frequency of 0.01. We only included the populations primarily studied in the GWASs: CEU (central European), ASW (African American) and JPT (Japanese). We assigned all SNPs in promoter-distal interactions to their interacting gene(s) ("target genes") using cardiomyocyte promoter capture Hi-C data. We did not require the SNP to map to regions associated with open chromatin or enhancer marks as these types of data are highly cell-type specific and we did not wish to exclude SNPs in regions that may be active in non-assayed cell types.

We note that one major GWAS for dilated cardiomyopathy was not included in the NHGRI-EBI database (Meder et al. 2014), likely because there is an error obtaining the online methods of the paper. After careful inspection of the study, we concluded that the GWAS met the NHGRI-EBI criteria and included the associations from that study in our analysis. A complete list of all studies used in this analysis can be found in Supplementary File 8.

MGI analysis

To calculate enrichment of target genes to cause cardiovascular phenotypes when deleted in mice (Mouse Genome Informatics database), we randomly selected 347 genes from the list of starting genes (i.e. genes with at least one promoter-distal interaction in CMs, meaning it could be a target gene), and calculated the proportion that caused a cardiovascular phenotype in mice. We performed this randomized selection for 100 iterations to generate the randomized (expected) values. Random genes were not required to be expressed, as the set of target genes contains genes that are not expressed. P-value was calculated with a Z test.

eQTL analysis

For eQTLs used in comparisons with GWAS variants and Hi-C interactions, we used the set of GTEx v7 eQTLs identified as significant in the left ventricle of the heart (Carithers et al. 2015). eQTLs were called significant if $q<0.05$ after false discovery rate correction (Storey and Tibshirani 2003). We only considered promoter-distal eQTLs that were at least 10 kb from their associated gene to allow for that eQTL to map to an interaction with it's associated gene.

To calculate enrichment for eQTLs to loop to their associated gene, we used a background model whereby each promoter's set of interactions were re-mapped to a different promoter, keeping the distance and strand orientation consistent. We performed this re-mapping of all promoter interactions 1000 times and calculated the proportion of all eQTLs that mapped to interactions for their eQTL-

890 associated gene in each permutation. We either used the CM interactions or the iPSC interactions with
891 the same set of left ventricle eQTLs to compare cell-type specificity of the promoter interaction data.

892 **Data Availability:**

893 Raw and processed sequencing data are provided at ArrayExpress through accession numbers E-
894 MTAB-6014 (Hi-C) and E-MTAB-6013 (RNA-seq).

895 **Acknowledgements**

896 We kindly thank the laboratory of Yoav Gilad for providing the iPSC line and assisting with the
897 cardiomyocyte differentiation protocol, and Dr. Kohta Ikegami for assistance with the ChIP-seq protocol.

898 **Competing Interests**

899 None

900 **Sources of Funding**

901 This work was supported by NIH grants HL123857 (M.A.N.), HL119967 (M.A.N.), HL118758 (M.A.N),
902 HL128075 (M.A.N. and E.M.M.), T32GMOO7197 (L.E.M.), American Heart Association Pre-doctoral
903 award 17PRE33410726 (L.E.M.), HL137307 (L.E.M).

904

905 **References**

906 Arking DE, Pulit SL, Crotti L, van der Harst P, Munroe PB, Koopmann TT, Sotoodehnia N, Rossin EJ,
907 Morley M, Wang X, Johnson AD, Lundby A, Gudbjartsson DF, Noseworthy PA, Eijgelsheim M,
908 Bradford Y, Tarasov K V, Dörr M, Müller-Nurasyid M, et al. 2014. Genetic association study of QT
909 interval highlights role for calcium signaling pathways in myocardial repolarization. *Nat Genet* **46**:
910 826–836.

911 Arnolds DE, Liu F, Fahrenbach JP, Kim GH, Schillinger KJ, Smemo S, McNally EM, Nobrega MA, Patel

912 V V., Moskowitz IP. 2012. TBX5 drives Scn5a expression to regulate cardiac conduction system
913 function. *J Clin Invest* **122**: 2509–2518.

914 Ashburner M, Ball CA, Blake JA, Botstein D, Butler H, Cherry JM, Davis AP, Dolinski K, Dwight SS,
915 Eppig JT, Harris MA, Hill DP, Issel-Tarver L, Kasarskis A, Lewis S, Matese JC, Richardson JE,
916 Ringwald M, Rubin GM, et al. 2000. Gene ontology: tool for the unification of biology. The Gene
917 Ontology Consortium. *Nat Genet* **25**: 25–9.

918 Banovich NE, Li YI, Raj A, Ward MC, Greenside P, Calderon D, Tung PY, Burnett JE, Myrthil M,
919 Thomas SM, Burrows CK, Romero IG, Pavlovic BJ, Kundaje A, Pritchard JK, Gilad Y. 2018.
920 Impact of regulatory variation across human iPSCs and differentiated cells. *Genome Res* **28**: 122–
921 131.

922 Blake JA, Eppig JT, Kadin JA, Richardson JE, Smith CL, Bult CJ, the Mouse Genome Database Group.
923 2017. Mouse Genome Database (MGD)-2017: community knowledge resource for the laboratory
924 mouse. *Nucleic Acids Res* **45**: D723–D729.

925 Burridge PW, Matsa E, Shukla P, Lin ZC, Churko JM, Ebert AD, Lan F, Diecke S, Huber B, Mordwinkin
926 NM, Plews JR, Abilez OJ, Cui B, Gold JD, Wu JC. 2014. Chemically defined generation of human
927 cardiomyocytes. *Nat Methods* **11**: 855–60.

928 Cai C-L, Zhou W, Yang L, Bu L, Qyang Y, Zhang X, Li X, Rosenfeld MG, Chen J, Evans S. 2005. T-box
929 genes coordinate regional rates of proliferation and regional specification during cardiogenesis.
930 *Development* **132**: 2475–2487.

931 Cairns J, Freire-Pritchett P, Wingett SW, Várnai C, Dimond A, Plagnol V, Zerbino D, Schoenfelder S,
932 Javierre B-M, Osborne C, Fraser P, Spivakov M. 2016. CHiCAGO: robust detection of DNA
933 looping interactions in Capture Hi-C data. *Genome Biol* **17**: 127.

934 Calo E, Wysocka J. 2013. Modification of enhancer chromatin: what, how, and why? *Mol Cell* **49**: 825–

935 37.

936 Carithers LJ, Ardlie K, Barcus M, Branton PA, Britton A, Buia SA, Compton CC, DeLuca DS, Peter-
937 Demchok J, Gelfand ET, Guan P, Korzeniewski GE, Lockhart NC, Rabiner CA, Rao AK, Robinson
938 KL, Roche N V., Sawyer SJ, Segrè A V., et al. 2015. A Novel Approach to High-Quality
939 Postmortem Tissue Procurement: The GTEx Project. *Biopreserv Biobank* **13**: 311–319.

940 Claussnitzer M, Dankel SN, Kim K-H, Quon G, Meuleman W, Haugen C, Glunk V, Sousa IS, Beaudry
941 JL, Puviindran V, Abdennur NA, Liu J, Svensson P-A, Hsu Y-H, Drucker DJ, Mellgren G, Hui C-C,
942 Hauner H, Kellis M. 2015. *FTO* Obesity Variant Circuitry and Adipocyte Browning in Humans. *N*
943 *Engl J Med* **373**: 895–907.

944 Cowper-Sal·lari R, Zhang X, Wright JB, Bailey SD, Cole MD, Eeckhoute J, Moore JH, Lupien M. 2012.
945 Breast cancer risk–associated SNPs modulate the affinity of chromatin for FOXA1 and alter gene
946 expression. *Nat Genet* **44**: 1191–1198.

947 Creyghton MP, Cheng AW, Welstead GG, Kooistra T, Carey BW, Steine EJ, Hanna J, Lodato MA,
948 Frampton GM, Sharp PA, Boyer LA, Young RA, Jaenisch R. 2010. Histone H3K27ac separates
949 active from poised enhancers and predicts developmental state. *Proc Natl Acad Sci* **107**: 21931–
950 21936.

951 Dao LTM, Galindo-Albarr?n AO, Castro-Mondragon JA, Andrieu-Soler C, Medina-Rivera A, Souaid C,
952 Charbonnier G, Griffon A, Vanhille L, Stephen T, Alomairi J, Martin D, Torres M, Fernandez N,
953 Soler E, van Helden J, Puthier D, Spicuglia S. 2017. Genome-wide characterization of mammalian
954 promoters with distal enhancer functions. *Nat Genet* **49**: 1073–1081.

955 Dekker J, Mirny L. 2016. The 3D Genome as Moderator of Chromosomal Communication. *Cell* **164**:
956 1110–1121.

957 Deng W, Lee J, Wang H, Miller J, Reik A, Gregory PD, Dean A, Blobel G a. 2012. Controlling long-

range genomic interactions at a native locus by targeted tethering of a looping factor. *Cell* **149**: 1233–1244.

Diao Y, Fang R, Li B, Meng Z, Yu J, Qiu Y, Lin KC, Huang H, Liu T, Marina RJ, Jung I, Shen Y, Guan K-L, Ren B. 2017. A tiling-deletion-based genetic screen for cis-regulatory element identification in mammalian cells. *Nat Methods* **14**: 629–635.

Dixon JR, Jung I, Selvaraj S, Shen Y, Antosiewicz-Bourget JE, Lee AY, Ye Z, Kim A, Rajagopal N, Xie W, Diao Y, Liang J, Zhao H, Lobanenkov V V, Ecker JR, Thomson JA, Ren B. 2015. Chromatin architecture reorganization during stem cell differentiation. *Nature* **518**.

Dixon JR, Selvaraj S, Yue F, Kim A, Li Y, Shen Y, Hu M, Liu JS, Ren B. 2012. Topological domains in mammalian genomes identified by analysis of chromatin interactions. *Nature* **485**: 376–380.

ENCODE Project Consortium TEP. 2012. An integrated encyclopedia of DNA elements in the human genome. *Nature* **489**: 57–74.

Erceg J, Pakozdi T, Marco-Ferreres R, Ghavi-Helm Y, Girardot C, Bracken AP, Furlong EEM. 2017. Dual functionality of cis-regulatory elements as developmental enhancers and Polycomb response elements. *Genes Dev* **31**: 590–602.

Franke M, Ibrahim DM, Andrey G, Schwarzer W, Heinrich V, Schöpflin R, Kraft K, Kempfer R, Jerković I, Chan W-L, Spielmann M, Timmermann B, Wittler L, Kurth I, Cambiaso P, Zuffardi O, Houge G, Lambie L, Brancati F, et al. 2016. Formation of new chromatin domains determines pathogenicity of genomic duplications. *Nature*.

Freire-Pritchett P, Schoenfelder S, Várnai C, Wingett SW, Cairns J, Collier AJ, García-Vílchez R, Furlan-Magaril M, Osborne CS, Fraser PJ, Rugg-Gunn PJ, Spivakov M. 2017. Global reorganisation of *cis* -regulatory units upon lineage commitment of human embryonic stem cells. *Elife* **6**: e21926.

981 Ghavi-Helm Y, Klein FA, Pakozdi T, Ciglar L, Noordermeer D, Huber W, Furlong EEM. 2014. Enhancer
982 loops appear stable during development and are associated with paused polymerase. *Nature* **512**:
983 96.

984 Gherghiceanu M, Barad L, Novak A, Reiter I, Itskovitz-Eldor J, Binah O, Popescu LM. 2011.
985 Cardiomyocytes derived from human embryonic and induced pluripotent stem cells: comparative
986 ultrastructure. *J Cell Mol Med* **15**: 2539–2551.

987 Gilbert N, Boyle S, Fiegler H, Woodfine K, Carter NP, Bickmore WA. 2004. Chromatin Architecture of
988 the Human Genome: Gene-Rich Domains Are Enriched in Open Chromatin Fibers. *Cell* **118**: 555–
989 566.

990 Gnirke A, Melnikov A, Maguire J, Rogov P, LeProust EM, Brockman W, Fennell T, Giannoukos G,
991 Fisher S, Russ C, Gabriel S, Jaffe DB, Lander ES, Nusbaum C. 2009. Solution hybrid selection
992 with ultra-long oligonucleotides for massively parallel targeted sequencing. *Nat Biotechnol* **27**:
993 182–9.

994 Guo D-C, Papke CL, Tran-Fadulu V, Regalado ES, Avidan N, Johnson RJ, Kim DH, Pannu H, Willing
995 MC, Sparks E, Pyeritz RE, Singh MN, Dalman RL, Grotta JC, Marian AJ, Boerwinkle EA, Frazier
996 LQ, LeMaire SA, Coselli JS, et al. 2009. Mutations in smooth muscle alpha-actin (ACTA2) cause
997 coronary artery disease, stroke, and Moyamoya disease, along with thoracic aortic disease. *Am J*
998 *Hum Genet* **84**: 617–27.

999 Heintzman ND, Hon GC, Hawkins RD, Kheradpour P, Stark A, Harp LF, Ye Z, Lee LK, Stuart RK,
1000 Ching CW, Ching KA, Antosiewicz-Bourget JE, Liu H, Zhang X, Green RD, Lobanenkov V V,
1001 Stewart R, Thomson JA, Crawford GE, et al. 2009. Histone modifications at human enhancers
1002 reflect global cell-type-specific gene expression. *Nature* **459**: 108–12.

1003 Heinz S, Benner C, Spann N, Bertolino E, Lin YC, Laslo P, Cheng JX, Murre C, Singh H, Glass CK.
1004 2010. Simple Combinations of Lineage-Determining Transcription Factors Prime cis-Regulatory

Elements Required for Macrophage and B Cell Identities. *Mol Cell* **38**: 576–589.

Hnisz D, Shrinivas K, Young RA, Chakraborty AK, Sharp PA. 2017. Perspective A Phase Separation Model for Transcriptional Control. *Cell* **169**: 13–23.

Javierre BM, Sewitz S, Cairns J, Wingett SW, Várnai C, Thiecke MJ, Freire-Pritchett P, Spivakov M, Fraser P, Burren OS, Cutler AJ, Todd JA, Wallace C, Wilder SP, Kreuzhuber R, Kostadima M, Zerbino DR, Stegle O, Kreuzhuber R, et al. 2016. Lineage-Specific Genome Architecture Links Enhancers and Non-coding Disease Variants to Target Gene Promoters. *Cell* **167**: 1369–1384.e19.

Jin F, Li Y, Dixon JR, Selvaraj S, Ye Z, Lee AY, Yen C-A, Schmitt AD, Espinoza C a, Ren B. 2013. A high-resolution map of the three-dimensional chromatin interactome in human cells. *Nature* **503**: 290–4.

Karakikes I, Ameen M, Termglinchan V, Wu JC. 2015. Human Induced Pluripotent Stem Cell–Derived Cardiomyocytes. *Circ Res* **117**.

Karlić R, Chung H-R, Lasserre J, Vlahovicek K, Vingron M. 2010. Histone modification levels are predictive for gene expression. *Proc Natl Acad Sci U S A* **107**: 2926–31.

Langmead B, Salzberg SL. 2012. Fast gapped-read alignment with Bowtie 2. *Nat Methods* **9**: 357–359.

Li H. 2011. Tabix: fast retrieval of sequence features from generic TAB-delimited files. *Bioinformatics* **27**: 718–9.

Lieberman-Aiden E, van Berkum NL, Williams L, Imakaev M, Ragoczy T, Telling A, Amit I, Lajoie BR, Sabo PJ, Dorschner MO, Sandstrom R, Bernstein B, Bender MA, Groudine M, Gnirke A, Stamatoyannopoulos J, Mirny LA, Lander ES, Dekker J. 2009. Comprehensive mapping of long-range interactions reveals folding principles of the human genome. *Science* **326**: 289–93.

Love MI, Huber W, Anders S. 2014. Moderated estimation of fold change and dispersion for RNA-seq

data with DESeq2. *Genome Biol* **15**: 550.

Lupiáñez DG, Kraft K, Heinrich V, Krawitz P, Brancati F, Klopocki E, Horn D, Kayserili H, Opitz JM, Laxova R, Santos-Simarro F, Gilbert-Dussardier B, Wittler L, Borschiwer M, Haas SA, Osterwalder M, Franke M, Timmermann B, Hecht J, et al. 2015. Disruptions of Topological Chromatin Domains Cause Pathogenic Rewiring of Gene-Enhancer Interactions. *Cell* **161**: 1012–1025.

Mahmoud AI, Kocabas F, Muralidhar SA, Kimura W, Koura AS, Thet S, Porrello ER, Sadek HA. 2013. Meis1 regulates postnatal cardiomyocyte cell cycle arrest. *Nature* **497**: 249–253.

Maurano MT, Humbert R, Rynes E, Thurman RE, Haugen E, Wang H, Reynolds AP, Sandstrom R, Qu H, Brody J, Shafer A, Neri F, Lee K, Kutyavin T, Stehling-Sun S, Johnson AK, Canfield TK, Giste E, Diegel M, et al. 2012. Systematic Localization of Common Disease-Associate Variation in Regulatorty DNA. *Science (80-)* **337**: 1190–1195.

Meder B, Rühle F, Weis T, Homuth G, Keller A, Franke J, Peil B, Lorenzo Bermejo J, Frese K, Huge A, Witten A, Vogel B, Haas J, Völker U, Ernst F, Teumer A, Ehlermann P, Zugck C, Friedrichs F, et al. 2014. A genome-wide association study identifies 6p21 as novel risk locus for dilated cardiomyopathy. *Eur Heart J* **35**: 1069–1077.

Miele A, Dekker J. 2008. Long-range chromosomal interactions and gene regulation. *Mol Biosyst* **4**: 1046.

Mifsud B, Tavares-Cadete F, Young AN, Sugar R, Schoenfelder S, Ferreira L, Wingett SW, Andrews S, Grey W, Ewels P a, Herman B, Happe S, Higgs A, LeProust E, Follows G a, Fraser P, Luscombe NM, Osborne CS. 2015. Mapping long-range promoter contacts in human cells with high-resolution capture Hi-C. *Nat Genet* **47**: 598–606.

Moshal K, Roder K, Werdich AA, Dural NT, Kim TY, Cooper LL, Lu YC, Choi B-R, Terentyev D, MacRae C, Koren G. 2017. LITAF, A Novel Regulator of Cardiac Excitation. *FASEB J* **31**: 686.3-

686.3.

Mumbach MR, Satpathy AT, Boyle EA, Dai C, Gowen BG, Cho SW, Nguyen ML, Rubin AJ, Granja JM, Kazane KR, Wei Y, Nguyen T, Greenside PG, Corces MR, Tycko J, Simeonov DR, Suliman N, Li R, Xu J, et al. 2017. Enhancer connectome in primary human cells identifies target genes of disease-associated DNA elements. *Nat Genet* **49**: 1602–1612.

Musunuru K, Strong A, Frank-Kamenetsky M, Lee NE, Ahfeldt T, Sachs K V, Li X, Li H, Kuperwasser N, Ruda VM, Pirruccello JP, Muchmore B, Prokunina-Olsson L, Hall JL, Schadt EE, Morales CR, Lund-Katz S, Phillips MC, Wong J, et al. 2010. From noncoding variant to phenotype via SORT1 at the 1p13 cholesterol locus. *Nature* **466**: 714–9.

Nikpay M, Goel A, Won H-H, Hall LM, Willenborg C, Kanoni S, Saleheen D, Kyriakou T, Nelson CP, Hopewell JC, Webb TR, Zeng L, Dehghan A, Alver M, Armasu SM, Auro K, Bjonnes A, Chasman DI, Chen S, et al. 2015. A comprehensive 1000 Genomes–based genome-wide association meta-analysis of coronary artery disease. *Nat Genet* **47**: 1121–1130.

Nora EP, Goloborodko A, Valton AL, Gibcus JH, Uebersohn A, Abdennur N, Dekker J, Mirny LA, Bruneau BG. 2017. Targeted Degradation of CTCF Decouples Local Insulation of Chromosome Domains from Genomic Compartmentalization. *Cell* **169**: 930–944.e22.

Nora EP, Lajoie BR, Schulz EG, Giorgetti L, Okamoto I, Servant N, Piolot T, van Berkum NL, Meisig J, Sedat J, Gribnau J, Barillot E, Blüthgen N, Dekker J, Heard E. 2012. Spatial partitioning of the regulatory landscape of the X-inactivation centre. *Nature* **485**: 381–385.

O'Leary NA, Wright MW, Brister JR, Ciufo S, Haddad D, McVeigh R, Rajput B, Robbertse B, Smith-White B, Ako-Adjei D, Astashyn A, Badretdin A, Bao Y, Blinkova O, Brover V, Chetvernin V, Choi J, Cox E, Ermolaeva O, et al. 2016. Reference sequence (RefSeq) database at NCBI: current status, taxonomic expansion, and functional annotation. *Nucleic Acids Res* **44**: D733-45.

1074 Patro R, Duggal G, Love MI, Irizarry RA, Kingsford C. 2017. Salmon provides fast and bias-aware
1075 quantification of transcript expression. *Nat Methods* **14**: 417–419.

1076 Pennacchio LA, Bickmore W, Dean A, Nobrega MA, Bejerano G. 2013. Enhancers: five essential
1077 questions. *Nat Rev Genet* **14**: 288–295.

1078 Petersen CM, Nielsen MS, Nykjaer A, Jacobsen L, Tommerup N, Rasmussen HH, Roigaard H,
1079 Gliemann J, Madsen P, Moestrup SK. 1997. Molecular identification of a novel candidate sorting
1080 receptor purified from human brain by receptor-associated protein affinity chromatography. *J Biol*
1081 *Chem* **272**: 3599–605.

1082 Phanstiel DH, Van Bortle K, Spacek D, Hess GT, Shamim MS, Machol I, Love MI, Aiden EL, Bassik
1083 MC, Snyder MP. 2017. Static and Dynamic DNA Loops form AP-1-Bound Activation Hubs during
1084 Macrophage Development. *Mol Cell* **67**: 1037–1048.e6.

1085 Phillips-Cremins JE, Sauria MEG, Sanyal A, Gerasimova TI, Lajoie BR, Bell JSK, Ong C-T, Hookway
1086 TA, Guo C, Sun Y, Bland MJ, Wagstaff W, Dalton S, McDevitt TC, Sen R, Dekker J, Taylor J,
1087 Corces VG. 2013. Architectural Protein Subclasses Shape 3D Organization of Genomes during
1088 Lineage Commitment. *Cell* **153**: 1281–1295.

1089 Phillips JE, Corces VG. 2009. CTCF: master weaver of the genome. *Cell* **137**: 1194–211.

1090 Pikkarainen S, Tokola H, Kerkelä R, Ruskoaho H. 2004. GATA transcription factors in the developing
1091 and adult heart. *Cardiovasc Res* **63**: 196–207.

1092 Purcell S, Neale B, Todd-Brown K, Thomas L, Ferreira MAR, Bender D, Maller J, Sklar P, de Bakker
1093 PIW, Daly MJ, Sham PC. 2007. PLINK: a tool set for whole-genome association and population-
1094 based linkage analyses. *Am J Hum Genet* **81**: 559–75.

1095 Quinlan AR, Hall IM. 2010. BEDTools: a flexible suite of utilities for comparing genomic features.
1096 *Bioinformatics* **26**: 841–2.

1097 Rada-Iglesias A, Bajpai R, Swigut T, Brugmann SA, Flynn RA, Wysocka J. 2011. A unique chromatin
1098 signature uncovers early developmental enhancers in humans. *Nature* **470**: 279–283.

1099 Rao SSP, Huntley MH, Durand NC, Stamenova EK, Bochkov ID, Robinson JT, Sanborn AL, Machol I,
1100 Omer AD, Lander ES, Aiden EL. 2014. A 3D Map of the Human Genome at Kilobase Resolution
1101 Reveals Principles of Chromatin Looping. *Cell* **159**: 1665–1680.

1102 Roadmap Epigenomics Consortium A, Kundaje A, Meuleman W, Ernst J, Bilenky M, Yen A, Heravi-
1103 Moussavi A, Kheradpour P, Zhang Z, Wang J, Ziller MJ, Amin V, Whitaker JW, Schultz MD, Ward
1104 LD, Sarkar A, Quon G, Sandstrom RS, Eaton ML, et al. 2015. Integrative analysis of 111 reference
1105 human epigenomes. *Nature* **518**: 317–30.

1106 Rubin AJ, Barajas BC, Furlan-Magaril M, Lopez-Pajares V, Mumbach MR, Howard I, Kim DS, Boxer
1107 LD, Cairns J, Spivakov M, Wingett SW, Shi M, Zhao Z, Greenleaf WJ, Kundaje A, Snyder M,
1108 Chang HY, Fraser P, Khavari PA. 2017. Lineage-specific dynamic and pre-established enhancer–
1109 promoter contacts cooperate in terminal differentiation. *Nat Genet*.

1110 Sakabe NJ, Aneas I, Shen T, Shokri L, Park S-Y, Bulyk ML, Evans SM, Nobrega MA. 2012. Dual
1111 transcriptional activator and repressor roles of TBX20 regulate adult cardiac structure and function.
1112 *Hum Mol Genet* **21**: 2194–2204.

1113 Schmitt AD, Hu M, Jung I, Xu Z, Qiu Y, Tan CL, Li Y, Lin S, Lin Y, Barr CL, Ren B. 2016. A
1114 Compendium of Chromatin Contact Maps Reveals Spatially Active Regions in the Human
1115 Genome. *Cell Rep* **17**: 2042–2059.

1116 Schoenfelder S, Furlan-Magaril M, Mifsud B, Tavares-Cadete F, Sugar R, Javierre B-M, Nagano T,
1117 Katsman Y, Sakthidevi M, Wingett SW, Dimitrova E, Dimond A, Edelman LB, Elderkin S, Tabbada
1118 K, Darbo E, Andrews S, Herman B, Higgs A, et al. 2015. The pluripotent regulatory circuitry
1119 connecting promoters to their long-range interacting elements. *Genome Res* **25**: 582–597.

1120 Shen T, Aneas I, Sakabe N, Dirschinger RJ, Wang G, Smemo S, Westlund JM, Cheng H, Dalton N, Gu
1121 Y, Boogerd CJ, Cai C, Peterson K, Chen J, Nobrega MA, Evans SM. 2011. Tbx20 regulates a
1122 genetic program essential to adult mouse cardiomyocyte function. *J Clin Invest* **121**: 4640–54.

1123 Shin H, Shi Y, Dai C, Tjong H, Gong K, Alber F, Zhou XJ. 2016. TopDom: an efficient and deterministic
1124 method for identifying topological domains in genomes. *Nucleic Acids Res* **44**: e70.

1125 Siersbæk R, Madsen JGS, Javierre BM, Nielsen R, Bagge EK, Cairns J, Wingett SW, Traynor S,
1126 Spivakov M, Fraser P, Mandrup S. 2017. Dynamic Rewiring of Promoter-Anchored Chromatin
1127 Loops during Adipocyte Differentiation. *Mol Cell* **66**: 420–435.e5.

1128 Smemo S, Campos LC, Moskowitz IP, Krieger JE, Pereira AC, Nobrega MA. 2012. Regulatory variation
1129 in a TBX5 enhancer leads to isolated congenital heart disease. *Hum Mol Genet* **21**: 3255–63.

1130 Smemo S, Tena JJ, Kim K-H, Gamazon ER, Sakabe NJ, Gómez-Marín C, Aneas I, Credidio FL,
1131 Sobreira DR, Wasserman NF, Lee JH, Puviindran V, Tam D, Shen M, Son JE, Vakili NA, Sung H-
1132 K, Naranjo S, Acemel RD, et al. 2014. Obesity-associated variants within FTO form long-range
1133 functional connections with IRX3. *Nature* **507**: 371–5.

1134 Smith NL, Felix JF, Morrison AC, Demissie S, Glazer NL, Loehr LR, Cupples LA, Dehghan A, Lumley
1135 T, Rosamond WD, Lieb W, Rivadeneira F, Bis JC, Folsom AR, Benjamin E, Aulchenko YS,
1136 Haritunians T, Couper D, Murabito J, et al. 2010. Association of Genome-Wide Variation With the
1137 Risk of Incident Heart Failure in Adults of European and African Ancestry: A Prospective Meta-
1138 Analysis From the Cohorts for Heart and Aging Research in Genomic Epidemiology (CHARGE)
1139 Consortium. *Circ Cardiovasc Genet* **3**: 256–266.

1140 Soneson C, Love MI, Robinson MD. 2015. Differential analyses for RNA-seq: transcript-level estimates
1141 improve gene-level inferences. *F1000Research* **4**: 1521.

1142 Speir ML, Zweig AS, Rosenbloom KR, Raney BJ, Paten B, Nejad P, Lee BT, Learned K, Karolchik D,

1143 Hinrichs AS, Heitner S, Harte RA, Haeussler M, Guruvadoo L, Fujita PA, Eisenhart C, Diekhans M,
1144 Clawson H, Casper J, et al. 2016. The UCSC Genome Browser database: 2016 update. *Nucleic*
1145 *Acids Res* **44**: D717–D725.

1146 Spitz F, Furlong EEM. 2012. Transcription factors: from enhancer binding to developmental control. *Nat*
1147 *Rev Genet* **13**: 613–626.

1148 Stevens TJ, Lando D, Basu S, Atkinson LP, Cao Y, Lee SF, Leeb M, Wohlfahrt KJ, Boucher W,
1149 O'Shaughnessy-Kirwan A, Cramard J, Faure AJ, Ralser M, Blanco E, Morey L, Sansó M, Palayret
1150 MGS, Lehner B, Di Croce L, et al. 2017. 3D structures of individual mammalian genomes studied
1151 by single-cell Hi-C. *Nature* **544**: 59–64.

1152 Storey JD, Tibshirani R. 2003. Statistical significance for genomewide studies. *Proc Natl Acad Sci U S*
1153 *A* **100**: 9440–5.

1154 Symmons O, Pan L, Remeseiro S, Aktas T, Klein F, Huber W, Spitz F. 2016. The Shh Topological
1155 Domain Facilitates the Action of Remote Enhancers by Reducing the Effects of Genomic
1156 Distances. *Dev Cell* **39**: 529–543.

1157 Tsujimura T, Klein FA, Langenfeld K, Glaser J, Huber W, Spitz F. 2015. A Discrete Transition Zone
1158 Organizes the Topological and Regulatory Autonomy of the Adjacent Tfap2c and Bmp7 Genes ed.
1159 W.A. Bickmore. *PLoS Genet* **11**: e1004897.

1160 Visel A, Minovitsky S, Dubchak I, Pennacchio LA. 2007. VISTA Enhancer Browser--a database of
1161 tissue-specific human enhancers. *Nucleic Acids Res* **35**: D88-92.

1162 Watt AJ, Battle MA, Li J, Duncan SA. 2004. GATA4 is essential for formation of the proepicardium and
1163 regulates cardiogenesis. *Proc Natl Acad Sci* **101**: 12573–12578.

1164 Wingett S, Ewels P, Furlan-Magaril M, Nagano T, Schoenfelder S, Fraser P, Andrews S. 2015. HiCUP:
1165 pipeline for mapping and processing Hi-C data. *F1000Research* **4**: 1310.

1166 Wright JB, Brown SJ, Cole MD. 2010. Upregulation of c-MYC in cis through a Large Chromatin Loop

1167 Linked to a Cancer Risk-Associated Single-Nucleotide Polymorphism in Colorectal Cancer Cells.

1168 *Mol Cell Biol* **30**: 1411–1420.

Figure 1 - Figure Supplement 1

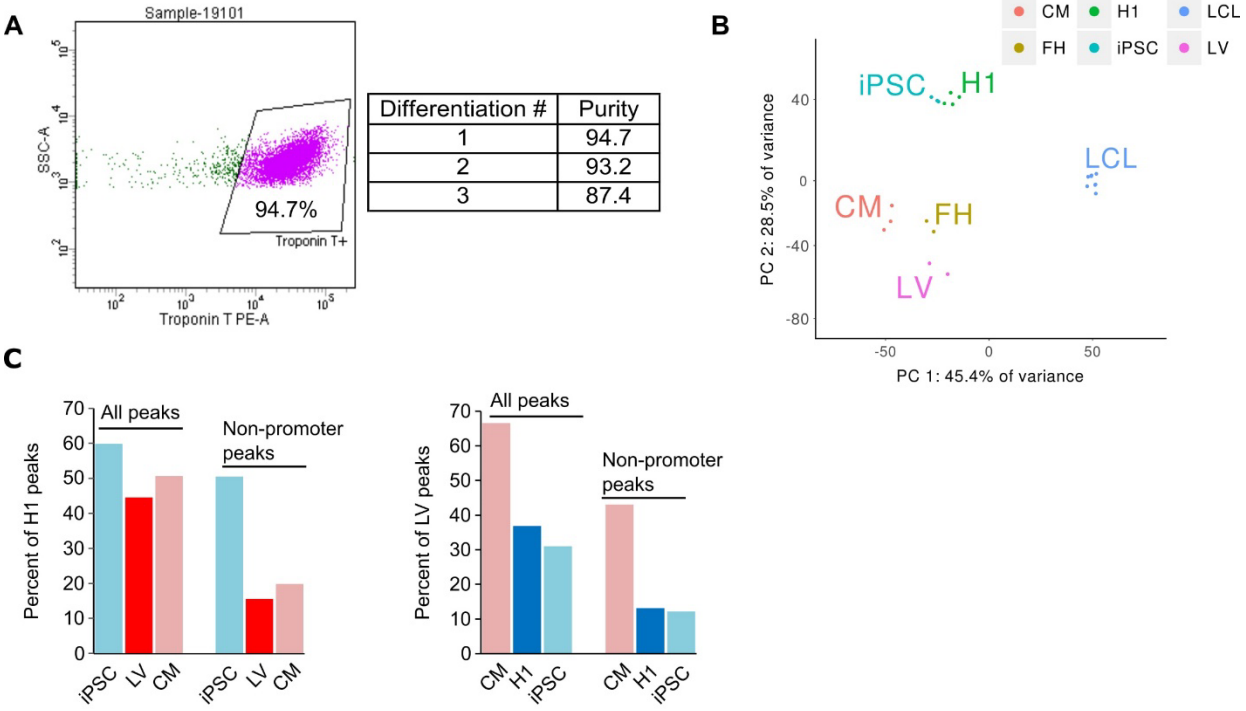

Differentiation #	Purity
1	94.7
2	93.2
3	87.4

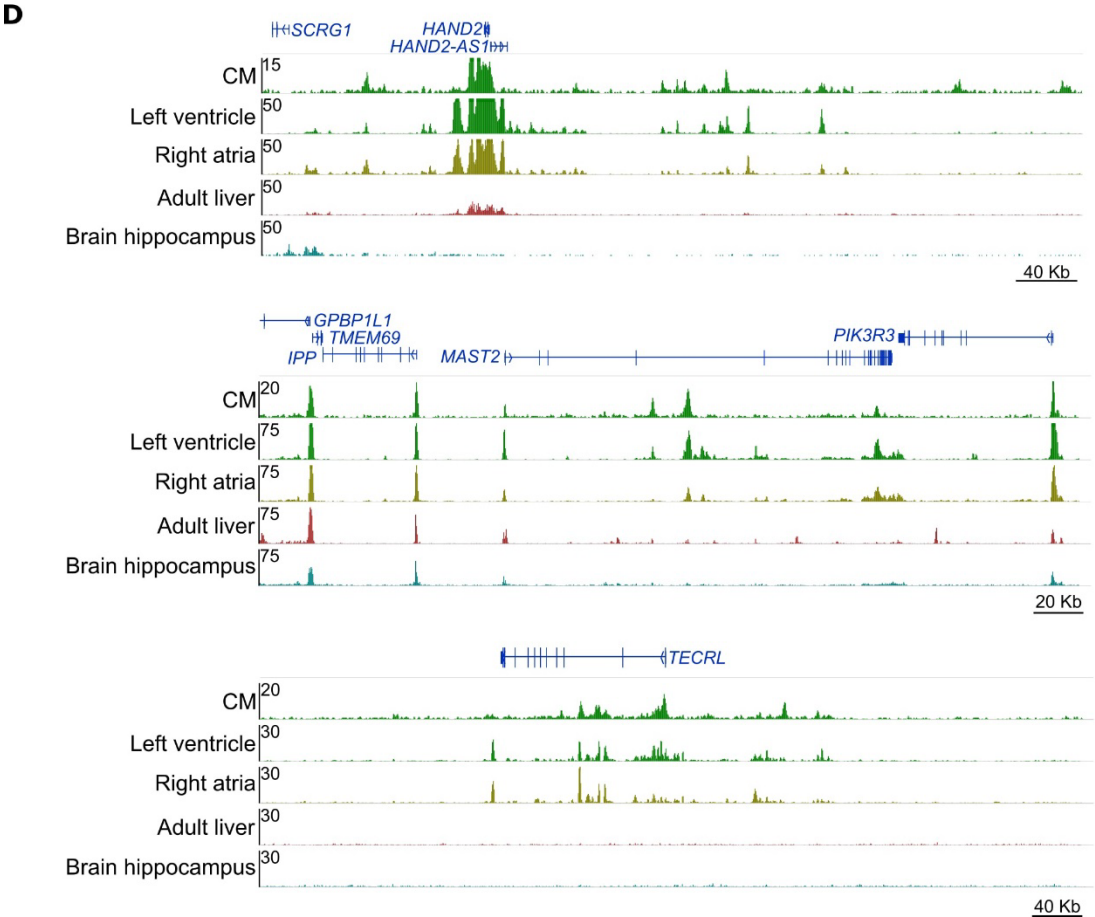

1169

Figure 1—figure supplement 1. **(A)** Flow cytometry of iPSC-derived cardiomyocytes. Representative image of flow data for cardiomyocytes (left) and percent cardiac troponin T (cTnT) positive for each differentiation (right). Cells were first gated on live/dead and then on cTnT staining. **(B)** Principle component analysis of RNA-seq data in iPSCs and CMs along with H1 embryonic stem cells, left ventricular cells (LV), fetal heart cells (FH), and lymphoblastoid cell line cells (LCL). LCLs cluster independently from iPSC and CM, indicating that iPSCs were faithfully reprogrammed. **(C)** Percentage of Epigenome Roadmap H3K27ac ChIP-seq peaks overlapping iPSC and CM H3K27ac peaks. Overlaps for all peaks and only non-promoter peaks are shown. LV, left ventricle; H1, H1 embryonic stem cell line. **(D)** Three genome browser snap-shots displaying the epigenetic landscape in CMs compared to left ventricle, right atria, adult liver and brain hippocampus from the Epigenome Roadmap.

Figure 1 - Figure Supplement 2

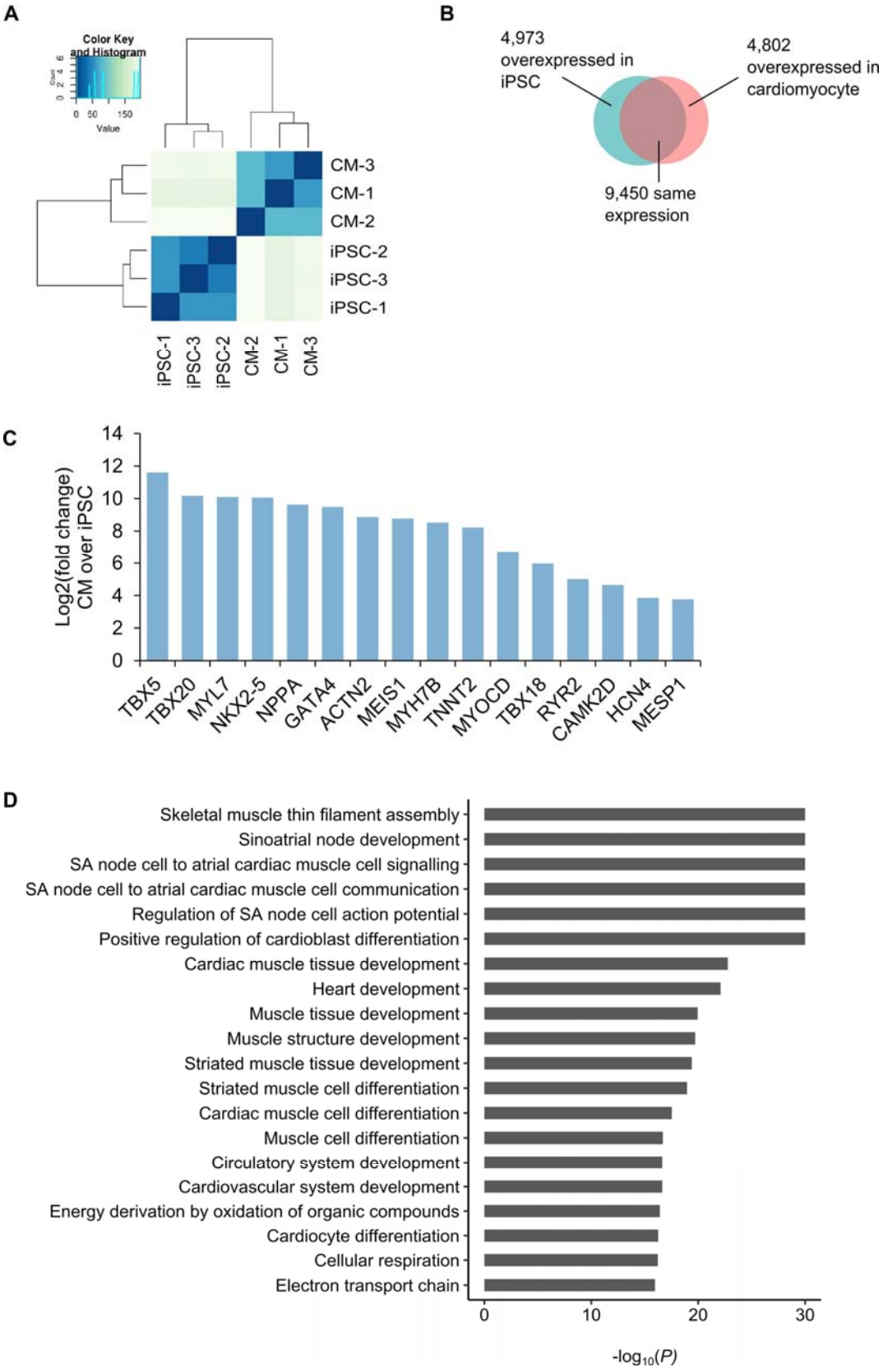

1180

Figure 1—figure supplement 2. (A) Cluster analysis of RNA-seq data from each triplicate of iPSC and CM. **(B)** Number of genes differentially expressed in each cell type. **(C)** Selected genes overexpressed in CMs relative to iPSCs. **(D)** Gene Ontology enrichment analysis of the biological processes associated with the 4,802 genes overexpressed in cardiomyocytes.

Figure 1 - Figure Supplement 3

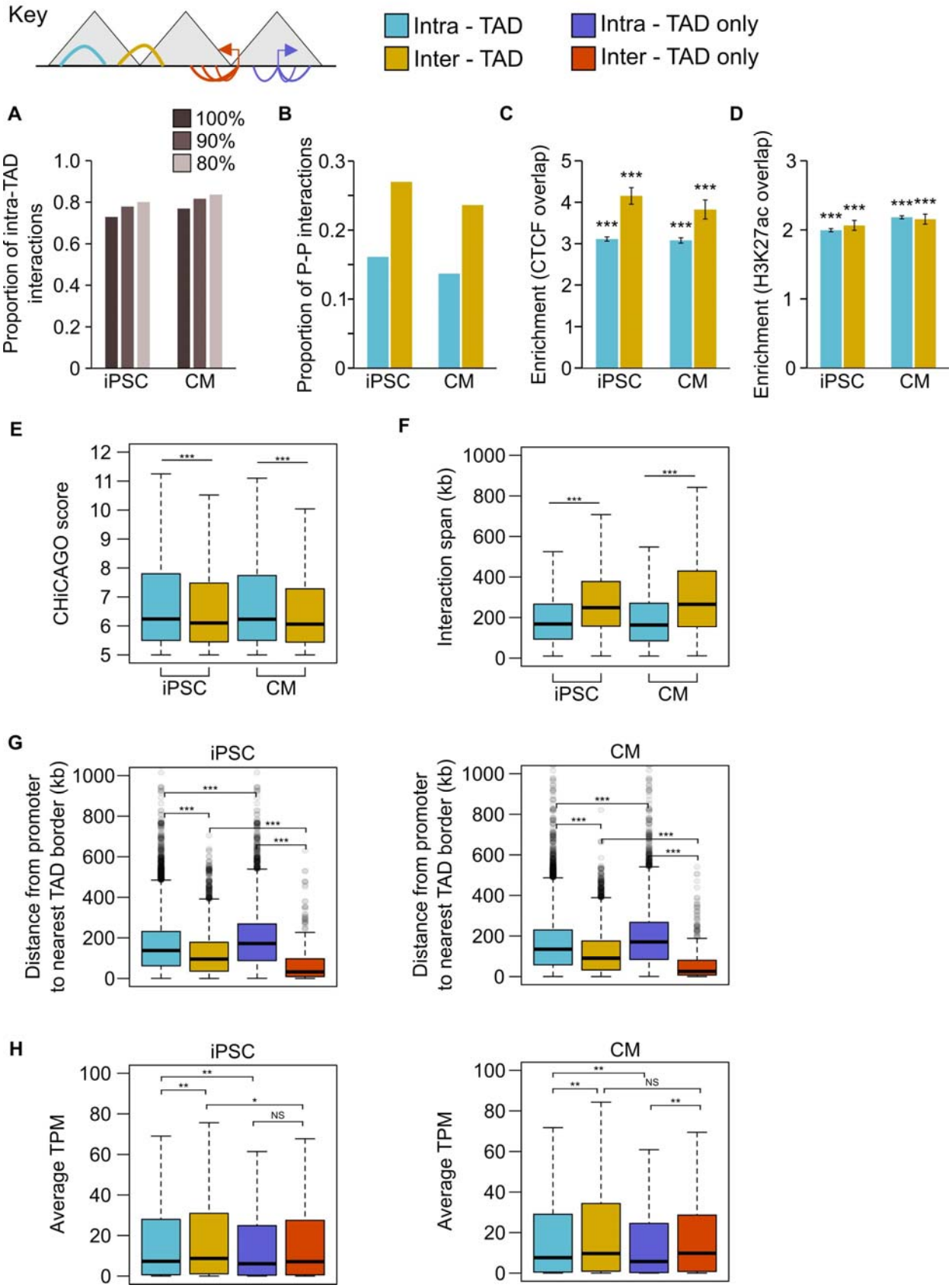

Figure 1—figure supplement 3. In this analysis, interactions were classified as intra-TAD (both ends of the interaction fully within a single TAD) or inter-TAD (each end of the interaction is in a different TAD). Interactions falling partially or wholly within TAD "boundaries" or "gaps" as defined by TopDom were omitted (see Methods). **(A)** Proportion of interactions that are intra-TAD at different cut-offs. All analyses used interactions that were 100% within a TAD. **(B)** Proportion of promoter-promoter interactions in the set of intra-TAD and inter-TAD interactions. **(C,D)** Fold enrichment for intra-TAD and inter-TAD interactions to overlap CTCF **(C)** or H3K27ac peaks **(D)**. Only promoter-distal ChIP-seq peaks were analyzed. ***$P < 2.2x10^{-16}$, Z-test. **(E)** CHiCAGO score and **(F)** interaction span of intra- vs. inter-TAD interactions. ***$P < 2.2x10^{-16}$, Wilcoxon rank-sum test. **(G,H)** Considering promoters with an intra-TAD interaction, an inter-TAD interaction, or exclusively intra-TAD or inter-TAD interactions: **(G)** distance from the promoter TSS to the nearest TAD boundary and **(H)** average TPM value of the promoter. ***$P < 2.2x10^{-16}$, **$P < 0.01$, *$P < 0.05$, NS = not significant, Wilcoxon rank-sum test.

Figure 3 - Figure Supplement 1

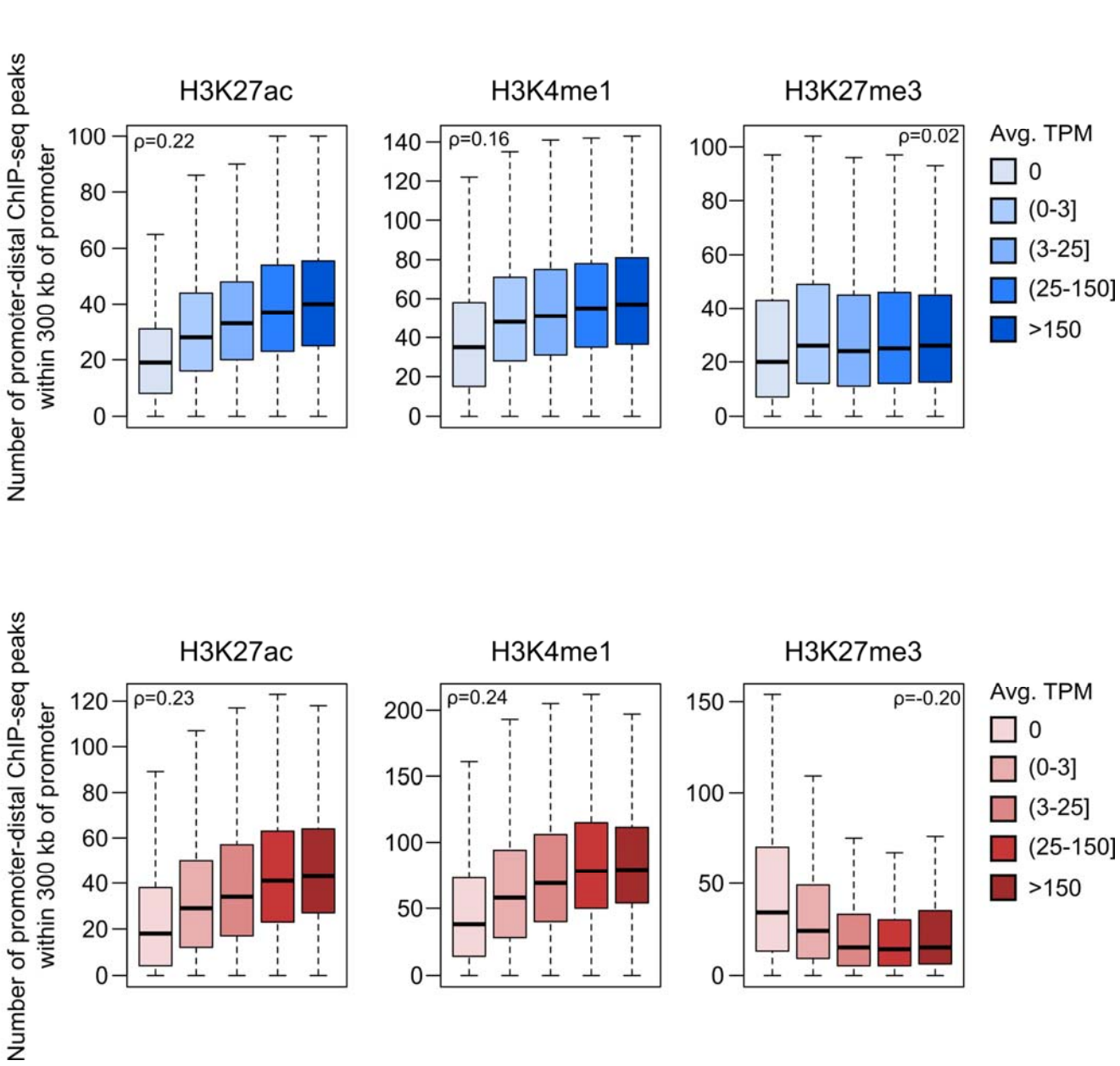

Figure 3—figure supplement 1. Number of promoter-distal histone ChIP-seq peaks within 300 kb of promoters in iPSC **(A)** and CM **(B)**. Spearman's rho (ρ) was calculated on the full set of promoter expression values/peak counts for all promoters with at least one significant interaction in the respective cell type (12,926 genes for iPSC and 13,555 genes for CM; see Methods). Data are grouped by expression category to emphasize the trend. Horizontal bars indicate the median for each

expression category. All correlation estimates are significant at $P < 2.2x10^{-16}$ except for H3K27me3 in iPSCs ($P = 0.06$).

Figure 4 - Figure Supplement 1

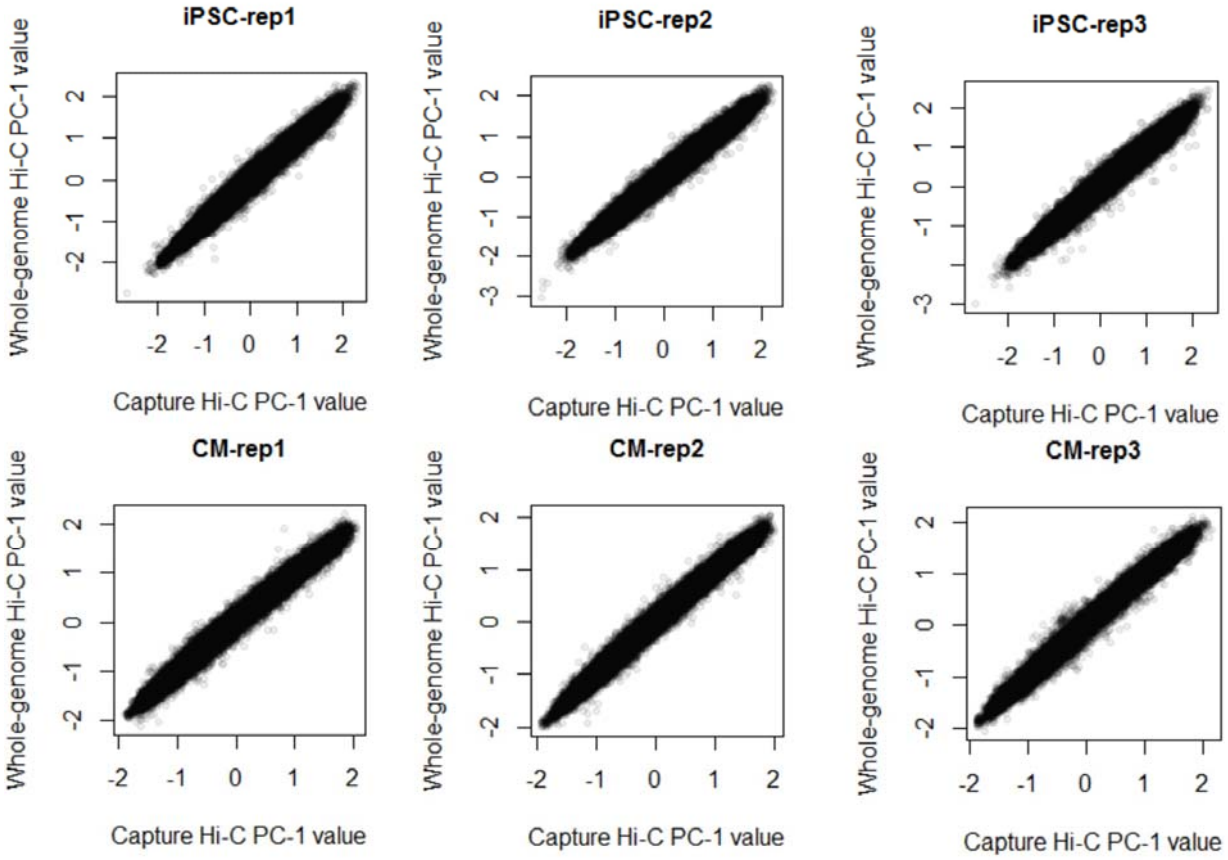

Figure 4—figure supplement 1. Correlation between the A/B compartment score (principle component analysis of interaction data, PC-1) in whole-genome Hi-C (y-axis) and promoter capture Hi-C (x-axis) in iPSCs (top) and CMs (bottom). Spearman's $\rho > 0.98$, $P < 2.2x10^{-16}$ in all cases.

Figure 4 - Figure Supplement 2

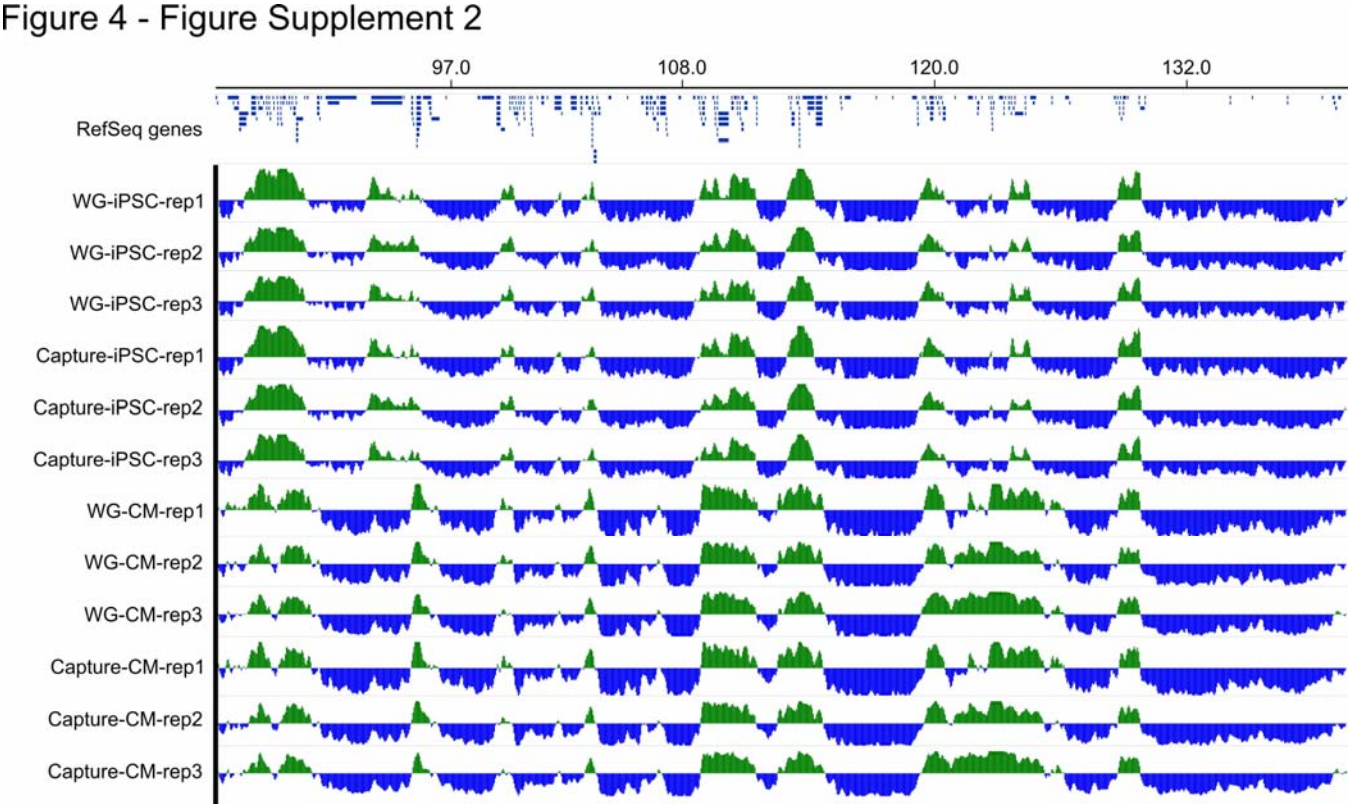

Figure 4—figure supplement 2. Genome browser snapshot of a ~53 Mb region on chromosome 4 showing A/B compartments in all three replicates of iPSCs and CMs using both whole-genome (WG) and promoter capture Hi-C data.

Figure 4 - Figure Supplement 3

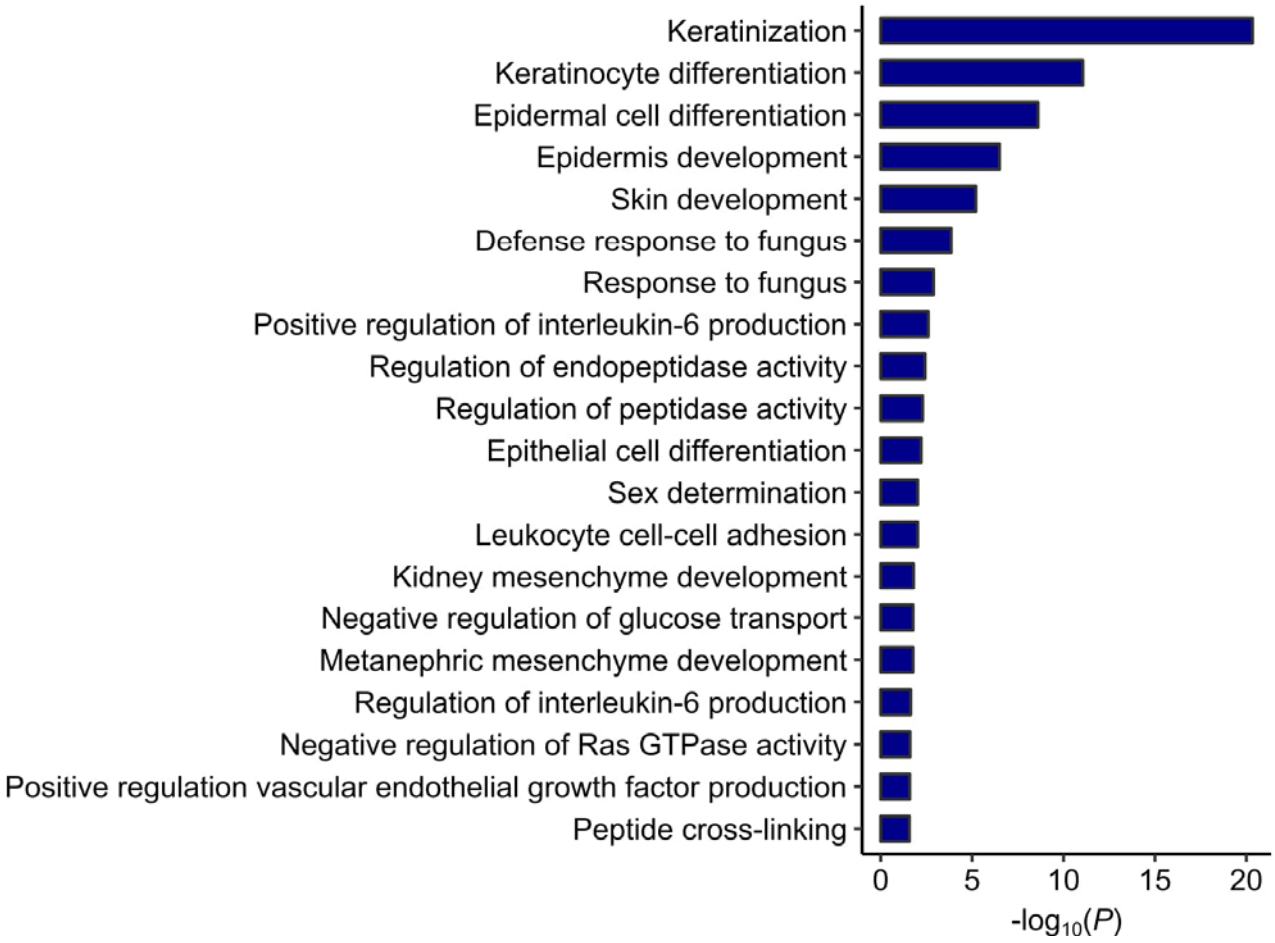

Figure 4—figure supplement 3. GO analysis on the genes switching from active A compartments in iPSCs to inactive B compartments in CMs.

Supplementary Movie 1 – Video of iPSC-derived cardiomyocytes exhibiting spontaneous beating at day 20 of the differentiation (day of cell harvesting).

Supplementary File Legends

Supplementary File 1 – PCHi-C interactions for iPSC. Significant interactions in iPSC (identified in at least two out of three replicates) are presented in paired bed format. Column 7 is the CHiCAGO score; Column 8 contains the gene information (gene name, identifier, strand, TSS position). If the interaction involves another promoter, the second gene name information is provided after the "|" symbol.

Supplementary File 2 – PCHi-C interactions for CM. Significant interactions in CM (identified in at least two out of three replicates) are presented in paired bed format. Column 7 is the CHiCAGO score; Column 8 contains the gene information (gene name, identifier, strand, TSS position). If the interaction involves another promoter, the second gene name information is provided after the "|" symbol.

Supplementary File 3 – CVD SNPs. All SNPs in high LD ($r^2 > 0.9$) with CVD tag SNPs are provided. The first 4 columns indicate the tag SNP position; columns 5-8 indicate the SNPs in LD with the tag SNP; column 9 is the degree of LD (r^2 value).

Supplementary File 4 – HOMER motif analysis for the distal interacting regions of promoter interactions. For each analysis presented in Figure 2, the full output of motifs identified in interacting fragments are listed.

Supplementary File 5 – Gene Ontology enrichment output. The full output of the GO enrichment analysis is provided.

Supplementary File 6 – Gene Ontology input gene lists. The list of genes used as input for GO analysis is provided.

Supplementary File 7 – GWAS terms used to compile studies. The list of trait terms used to filter GWAS studies is provided.

Supplementary File 8 – GWAS summary table. Table 8.1 contains information related to the CVD GWAS used in this paper, including PubMed ID, first author, date of publication, journal, study title, tag SNP chromosome position, rsID, trait. Table 8.2 contains information on each LD SNP-target gene interaction (tag SNP and corresponding LD SNP, target gene, interaction coordinates, target gene expression in iPSC and CM, MGI cardiovascular phenotype information.

Supplementary File 9 – Hi-C read information. Table 9.1 contains the probe sequences used for promoter capture, along with the corresponding gene name. Table 9.2 contains the total number of sequenced and processed/filtered reads for each Hi-C experiment. Table 9.3 contains the number of reads mapping to each promoter and the corresponding number of significant (present in at least two replicates) interactions called.

Supplementary File 10 – Public datasets used. ChIP-seq and RNA-seq datasets used in our analyses are listed.